International Journal of Nanomedicine

Dovepress
Taylor & Francis Group

Open Access Full Text Article

ORIGINAL RESEARCH

Combinatorial Anti-Mitotic Activity of Loratadine/5-Fluorouracil Loaded Zein Tannic Acid Nanoparticles in Breast Cancer Therapy: In silico, in vitro and Cell Studies

Mohamed Hamdi[1,2], Moawia M Al-Tabakha[3,4], Isra H Ali[1,5], Islam A Khalil[6]

[1]Department of Pharmaceutics, Faculty of Pharmacy, University of Sadat City, Sadat City, Egypt; [2]Nanomedicine Laboratory, Faculty of Pharmacy, University of Sadat City, Sadat City, Egypt; [3]Department of Pharmaceutical Sciences, College of Pharmacy and Health Sciences, Ajman University, Ajman, United Arab Emirates; [4]Centre of Medical and Bio-Allied Health Sciences Research Centre, Ajman University, Ajman, United Arab Emirates; [5]Department of Cardiovascular Medicine, Mayo Clinic, Rochester, MN, USA; [6]Department of Pharmaceutics, College of Pharmaceutical Sciences and Drug Manufacturing, Misr University for Science and Technology, 6th of October City, Giza, 12582, Egypt

Correspondence: Islam A Khalil, Department of Pharmaceutics, College of Pharmaceutical Sciences and Drug Manufacturing, Misr University of Science and Technology, 6th of October City, Giza, 12582, Egypt, Tel +201090140748, Email islam.khalil@must.edu.eg; islamkhll@gmail.com; Moawia M Al-Tabakha, Department of Pharmaceutical Sciences, College of Pharmacy and Health Sciences, Ajman University, P.O. Box 346, Ajman, United Arab Emirates, Tel +97167056208, Email m.altabakha@ajman.ac.ae

Introduction: Chemotherapy, the first approach in breast cancer management, is limited owing to systemic toxicity and drug resistance. For instance, 5-fluorouracil in recommended doses cause severe side effects, highlighting the urgent necessity of finding more effective and safer combinations. Hence, this study aims to develop biocompatible natural-based nanocarriers for the co-delivery of loratadine, an antihistaminic drug along with 5-fluorouracil in order to enhance the anticancer efficacy while reducing the required dose of 5-fluorouracil.

Methods: In silico virtual screening was performed to examine the probable molecular interactions between loratadine or 5-fluorouracil, individually with two different polymers, chitosan and zein, to determine the most suitable carrier system. Zein exhibited superior binding affinity compared to chitosan. Nanoparticle optimization was conducted using a Box-Behnken design with zein, tannic acid, and either loratadine or 5-fluorouracil concentration as independent variables. The optimized formulations were characterized by dynamic light scattering, entrapment efficiency, morphology, in-vitro release, followed by cytotoxicity, apoptosis, and cell-cycle analyses in MCF-7 cells.

Results: The optimal formulation consisted of zein (50 mg), tannic acid (131.93 mg), and loratadine or 5-fluorouracil (5 mg). The optimized formulation of Loratadine loaded nanoparticles (NPs) showed a particle size of 197 nm, polydispersity index (PDI) of 0.153, zeta potential of –21.78 mV, and entrapment efficiency of 61.33%. Furthermore, the optimized 5-fluorouracil loaded nanoparticles exhibited a particle size of 231 nm, 0.170 for PDI, zeta potential of –24.01 mV, and EE of 74.91% for entrapment efficiency. The sustained drug release profile exhibited a controlled pattern over 24–48 h. Flow cytometry results showed that the mixed nanoparticles exhibited potent cytotoxicity equivalent to 5-fluorouracil loaded nanoparticles alone despite containing only half the 5-fluorouracil dose, confirming a potential synergistic effect.

Conclusion: These findings confirmed the potential of drug-loaded nanoparticles as promising drug delivery systems for breast cancer management.

Keywords: in silico, loratadine, 5-fluorouracil, zein, tannic acid

Introduction

Cancer is considered to be one of the most significant contributors to increasing mortality rates worldwide. Breast cancer is the most common type of cancer in women worldwide. According to World Health Organization (WHO) reports,

https://doi.org/10.2147/IJN.S564050
Received: 29 August 2025
Accepted: 1 January 2026
Published: 15 January 2026

approximately 13% of women worldwide are diagnosed with breast cancer. Breast cancer is considered to be the primary cause of 3% of women deaths all over the world.[1–3]

Recently, some studies have shown that anti-histaminic drugs, such as loratadine (LOR), may exhibit potential anti-proliferative activity in cancer treatment when used alone or in combination therapy.[4,5] Generally, anti-histaminic drugs compete with histamine H1 receptor binding, resulting in blockage of histamine receptor toward histamine.[6] Consequently, antihistaminic medications can suppress tumor growth, development, and progression.[7,8]

Various studies have reported the efficacy of LOR as an anti-proliferative medication. For instance, a study conducted by Chen et al demonstrated the ability of LOR to stimulate cell cycle arrest in the G2/M phase during colon cancer treatment through three successive mechanisms: (a) checkpoint kinase 1 overexpression, (b) cell division cycle 25 inhibition (CDC 25), and (c) pro-apoptotic protein inactivation, resulting in caspase 9 (Casp-9) stimulated apoptosis.[9] Furthermore, Soul et al investigated the impact of pretreatment of cancer patients with LOR, which enhanced sensitivity toward radiotherapy.[5]

Fluoropyrimidines, mainly 5-Florouracil (5-FU), are commonly used for solid tumor management as in breast and colorectal cancer. 5-FU is considered as one of the most widely used chemotherapy in the management of breast and colorectal cancer, however, its clinical response rate rarely exceeds 10–15% when administered as a single therapy. This limitation returns back to the development of cellular resistance that retards its potential cytotoxicity. The primary resistance mechanism is attributed to the overexpression of thymidylate synthase (TYMS), which in turn reduces the binding affinity of 5-FU's active metabolite (5-FdUMP), and consequently the restoration of DNA synthesis. Other factors include dihydropyrimidine dehydrogenase (DPD) upregulation, which is the main enzyme that is responsible for 5-FU catabolism, as well as the reduced activity of both orotate phosphoribosyltransferase (OPRT) and thymidine phosphorylase (TP), thereby limiting the intracellular drug activation. Furthermore, resistant cancer cells demonstrate elevated DNA repair capacity and dysregulated apoptosis through p53 suppression and Bcl-2 overexpression, increasing survival rate despite the DNA damage. Therefore, a combinatory therapy with other drugs is studied in terms of modulating apoptotic and cell-cycle regulatory pathways to increase sensitization of tumor cells.[10] For instance, LOR, a second-generation antihistamine, has demonstrated anti-proliferative effects through inhibition of checkpoint kinase pathways, resulting in cell-cycle arrest at the G_2/M phase and induction of caspase-9-mediated apoptosis. On the other hand, 5-FU, a pyrimidine analog, interferes with DNA synthesis by forming a stable ternary complex with thymidylate synthase (TYMS), leading to DNA fragmentation and S-phase arrest. Hence, upon combination, complementary anti-mitotic activities can be achieved, where LOR enhances apoptotic activity and cell-cycle checkpoint activation, while 5-FU inhibits DNA synthesis. This dual mechanism is expected to enhance cytotoxicity at minimized chemotherapeutic doses, reducing systemic side effects associated with high doses 5-FU single therapy.

Zein (ZN) is the main protein found in corn and maize and is composed of various peptides with different molecular weights. These peptides are categorized as a) α-zein possessing two bands with an average molecular weight of 22–24 kDa, b) β-zein with an average molecular weight of 17 kDa, c) γ-ZN possessing two bands with an average molecular weight of 18–27 kDa, and d) δ-ZN with an average molecular weight of 10 kDa.[11]

ZN possesses many nonpolar (uncharged) amino acids within its structure, such as alanine (10%), proline (10%), leucine (20%), and glutamine (21–26%) rendering it of low water solubility. However, it has good film formation ability and encapsulation efficiency. Hence, the addition of alcohol, urea, or anionic surfactants is mandatory to increase the water solubility.[12,13] ZN is a promising naturally derived biomaterial in biomedical and pharmaceutical fields and can be efficiently utilized in the preparation of drug delivery systems for various bioactive cargoes. This is because of their high biocompatibility, good biodegradability, enhanced oral bioavailability, increased drug stability, controlled drug release, and improved drug targeting. Hence, it can introduce almost all the required properties of a promising nanocarrier system.[13,14]

Different approaches have been used to develop ZN nanoparticles (NPs), such as antisolvents, electrospraying, evaporation-induced self-assembly, and heat-induced self-assembly. Although they seem different, these methods possess a common mechanism, in which ZN is dissolved in hydroalcoholic solutions before being poured into water. Hence, changing the polarity of the medium from hydrophobic to hydrophilic causes the aggregation of ZN molecules, forming nanoparticles through hydrophobic interactions. It has also been reported that shear rate, ethanol concentration, and ZN

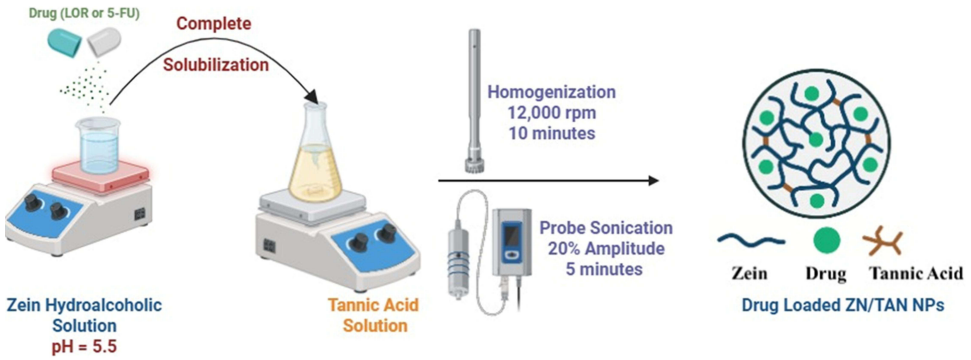

Scheme 1 Schematic Diagram for Preparation of Drug Loaded ZN/TAN NPs.

concentration may affect the size of the produced nanoparticles.[15] It is also worth mentioning that the chemical structure of ZN contains many amino, carboxyl, and hydroxyl groups, which renders it a promising platform for incorporating both hydrophobic and hydrophilic drugs using cross-linking agents, increasing entrapment efficiency.[12]

Tannic acid (TAN) is a hydrolyzable phenolic compound composed of a pentagalloyl glucose core surrounded by gallic acid molecules through ester bond linkages. TAN acts as an effective natural crosslinking agent owing to its multiple carbonyl and hydroxyl functional groups capable of formation of hydrogen bonding and hydrophobic–hydrophobic interactions with zein peptide backbone. These interactions stabilize the nanoparticles formation by reducing their aggregation while enhancing their sustained drug release. Furthermore, TAN exhibits some anticancer activity through caspase activation and ROS generation. In addition, it provides a synergistic biological role along with its crosslinking function.[16] Moreover, TAN has shown a confirmed capability to stimulate apoptosis in various cancer cells including the MCF-7 human breast cancer cell line.[17–19] This demonstrates that TAN-based nanoformulations can act as targeted drug delivery systems for breast cancer cells. Various studies using flow cytometry have illustrated that TAN apoptotic activity depends mainly on its ability to activate caspase signaling cascades in TAN-treated MCF-7 breast cancer cells.[16,20,21]

Therefore, this study aimed to investigate the activities of both LOR and 5-FU using in silico molecular docking. Both drugs were loaded individually into ZN nanoparticles using tannic acid as a crosslinking agent (ZN/TAN NPs) as shown in Scheme 1. Optimization of the developed nanoformulations was performed using the Box Behnken Design (BBD), where the studied variables were ZN concentration, drug amount, and tannic acid amount. On the other hand, the considered responses were selected to be nanoparticles size (nm), polydispersity index (PDI), zeta potential (ZP) as well as entrapment efficiency (EE%). The in-vitro assessments involved the investigation of both drug entrapment efficiency and drug release profiles. In-vitro cell line experiments were carried out to evaluate cytotoxicity and to calculate the IC_{50} values for free 5-FU, ZN/TAN NPs, LOR-ZN/TAN NPs, 5-FU-ZN/TAN NPs, and the combination of both drug-loaded ZN/TAN NPs (1:1 ratio). Finally, necrosis, apoptosis, and cell cycle analyses were performed to investigate the anticancer mechanism of the developed nanoformulations.

Materials and Methods

Materials

Zein, tannic acid, absolute ethanol (99%), cellulose dialysis membranes (cut-off 12,000 MW), Tween 80, and polyethylene glycol 400 (PEG 400) were purchased from Sigma Aldrich, Germany. Phosphate-buffered saline (PBS; pH 5.5) and 5-Florouracil were purchased from Acros (Belgium). Loratadine was a gift from Amoun Pharmaceutical Co. (Egypt). Human breast adenocarcinoma cell lines (MCF-7 and HTB-22) were obtained from American Type Culture Collection (ATCC, VA, USA).

https://doi.org/10.2147/IJN.S564050

In-silico Studies

Ligands and Polymers Files Preparation

The in silico investigations of this study aimed to examine the molecular interaction of two selected drugs, loratadine (LOR) and 5-Fluorouracil (5-FU), with two naturally derived polymers, Zein and Chitosan, to select the most appropriate polymeric carrier for nanoparticle preparation.

The structures of LOR and 5-FU were obtained in their minimized energy forms as SDF files from the PubChem database (https://pubchem.ncbi.nlm.nih.gov/). Furthermore, Zein and Chitosan structures were retrieved from the SWISS-MODEL repository (https://swissmodel.expasy.org/) and PDB database (https://www.rcsb.org/).[22,23]

Afterward, the polymer structures were further processed using PyMOL software to remove any co-crystallized ligands and water molecules while adding hydrogen atoms. Finally, the output files were used as PDB for docking analysis.

Molecular Docking

Molecular docking was performed using the CB-Dock 2.0 web server (http://clab.labshare.cn/cb-dock/php/index.php) to determine the molecular interactions and binding affinities between each individual drug from one side and each of the selected polymers on the other side. CB-Dock2 server performs modeling calculations through cavity-based docking. First, protein cavities are identified, then refined, making them more reliable than blind-docking approaches. The CB-Dock2 server also integrates AutoDock Vina scoring along with its automatic optimization for each cavity search box. This improves the accuracy and reproducibility of the modelling results compared to those obtained from standalone AutoDock Vina runs. For each drug–polymer interaction, the five top-ranked poses were determined, where the pocket pose possessing the lowest binding energy while the largest volume was selected. Furthermore, RMSD values for the top five selected poses were investigated, and only stable poses possessing RMSD < 2.0 Å were selected.[24]

Molecular Interaction Analysis and Visualization

The best interaction profile for each drug complex was further analyzed and visualized using BIOVIA Discovery Studio Visualizer (v19.1). The various molecular interactions include carbon–hydrogen bonding, conventional hydrogen bonding, π–alkyl and alkyl interactions, π–π stacking, and salt-bridge/electrostatic interactions. In addition, the amino acid residues involved in binding, as well as the distance, were determined. To display the binding behavior of polymer–drug complexes, 2D interaction diagrams were plotted to visualize them clearly.

Nanoparticles: Optimization, Development and Characterization

Preliminary Screening of Formulation Variables

To optimize the preparation of drug-loaded ZN/TAN nanoparticles (NPs), an initial screening was carried out to determine the influence of key preparation variables, such as formulation step sequence, aqueous phase volume, and homogenization/sonication, on formulation attributes, such as particle size, polydispersity index (PDI), surface charge, and entrapment efficiency.

Preliminary screening was performed using 5-FU alone, and not with LOR. This resulted in differences in the physicochemical properties of the two drugs. For instance, 5-FU is a hydrophilic drug with low molecular weight. Hence, it is expected to have a high tendency to diffuse out of the polymeric matrices during zein nanoparticle preparation, resulting in poor entrapment efficiency. In contrast, LOR is a hydrophobic drug with a high binding affinity toward zein's hydrophobic cavities within its protein matrices, resulting in a high capability of drug incorporation within the polymeric matrices during the formulation procedures. Therefore, the preparation of 5-FU loaded zein/tannic acid nanoparticles FU-ZN/TAN NPs exhibited greater preparation challenges than the loratadine-loaded zein/tannic acid nanoparticles LOR-ZN/TAN NPs.

This was also supported by the results obtained from the in silico studies, where it was found that LOR possesses a higher affinity than 5-FU toward complexation with zein, suggesting a higher liability of LOR for higher entrapment efficiency. Thus, 5-FU was selected for preliminary screening studies following the rationale that determining the variables that could enhance the entrapment efficiency of hydrophilic drugs, such as 5-FU, within zein matrices would also enhance the efficiency of hydrophobic drugs, such as LOR.

The FU-ZN/TAN NPs were prepared using the electrostatic complexation method, as reported previously, with some amendments.[25] Six formulations (F1–F6) were prepared, and 5 mg of 5-FU was dissolved in 5 mL of 1% zein hydroalcoholic solution. Afterward, the polymer-drug solution was added dropwise to a deionized tannic acid solution (F1 and F2) or water (F3 and F4). In the other formulations (F5 and F6), tannic acid solution was added to the polymer-drug solution as an antisolvent. Furthermore, some formulations (F1, F3, and F5) were subjected to homogenization at 12,000 rpm for 10 min, followed by probe sonication for 5 min for consecutive cycles (10 s on and 5 s off) at 20% amplitude, whereas the other samples (F2, F4, and F6) were collected after magnetic stirring. All preparations were formulated at ambient temperature, centrifuged for 15 minutes at 12000 rpm and 4°C before being collected, and washed (3x) using distilled water. Finally, the formulations were collected and resuspended in PBS for further analyses. For instance, the developed formulations were investigated in terms of particle size, polydispersity index (PDI), surface charge, and entrapment efficiency (EE%) to determine the most appropriate formulation conditions before developing the experimental design using Design Expert software.

Experimental Design

LOR-ZN/TAN NPs and FU-ZN/TAN NPs were prepared through a hydrogen bonding assisted complexation procedure, as reported previously with some modifications.[25] ZN solution was prepared under slight acidic conditions (pH 5.5) to ensure partial protonation of zein peptide backbone and effective phenolic interaction of tannic acid. The required amount of zein powder was dissolved in an 80% v/v aqueous ethanol solution to prepare the required concentration, as mentioned in Section 2.3.1. Then the pH was adjusted at 5.5 using few drops of acetic acid. Subsequently, a determined amount of either LOR or FU was added to the clear zein solution to prepare the corresponding NPs. Finally, the zein/drug solution was slowly added dropwise to 15 mL of the corresponding tannic acid solution while stirring. Afterward, the prepared formulations were homogenized (12,000 rpm, 10 min) and probe-sonicated (20% amplitude, 5 min, 10 s on/off), as explained in section 2.3.1, before being collected through centrifugation, washed, resuspended in PBS pH 7.4 and stored for further analysis and characterization.

Various factors that are believed to affect the properties of the developed NPs such were studied using Design Expert software (Version 13, Stat-Ease Inc., Suite 480 Minneapolis, MN 55413) through a Box-Behnken design (BBD), which was built to determine the optimized variables for the preparation of both LOR-ZN/TAN NPs and FU-ZN/TAN NPs, as shown in Table 1.

Table 1 Experimental Design for Optimization of Loratadine Loaded Zein Tannic Acid Nanoparticles and 5-Fluorouracil Loaded Zein Tannic Acid Nanoparticles

Factors	Levels	
	Low	High
X1: Zein (mg)	25	100
X2: Tannin acid (mg)	50	200
X3: LOR or FU (mg)	2.5	10
Evaluated responses	Desirability constraints	
Y1: Size (nm)	Minimize	
Y2: PDI	Minimize	
Y3: Charge (absolute) (mV)	Maximize	
Y4: EE (%)	Maximize	

Abbreviations: LOR, Loratadine; FU, 5-Flourouracil; PDI, Polydispersity index; EE, Entrapment Efficiency.

https://doi.org/10.2147/IJN.S564050

The amounts of zein, drug (LOR or 5-FU), and tannic acid are considered the most important variables that should be investigated to determine their influence on the properties of NPs. Hence, the independent variables were selected as X1: ZN amount (mg) dissolved in hydroalcoholic solution, X2: TAN amount (mg) dissolved in 15 mL of 0.001% v/v Tween solution in distilled water, and X3: LOR/FU amount (mg) dissolved in the corresponding 5 mL zein solution. On the other hand, the tested dependent variables were Y1: NPs size (nm), Y2: PDI, Y3: zeta potential (mV) and Y4: EE%. Nanoparticle preparation conditions, along with both low and high levels for each tested variable, were chosen based on preliminary screening studies described in Section 2.3.1. For example, the amounts of ZN selected were 25, 62.5, and 100 mg solubilized in 5 mL of a hydroalcoholic solution. The selected TAN amounts were 50, 125, and 200 mg dissolved in 15 mL of 0.001% v/v Tween solution. Finally, either the LOR or FU amounts were selected as 2.5 mg, 6.25 mg and 10 mg to be dissolved in the corresponding zein solution. The designed BBD was constructed to include 17 preparations as shown in Table 2.

All NPs were prepared as described in the previous sections. Both numerical and graphical optimization approaches were followed to achieve the highest desirability using the selected range of independent variables. Afterward, the credibility of the variable range was confirmed through the design space for each response.[26] In addition, interval estimates were used to determine outcomes.[27] Finally, the model validation was evaluated by calculating the bias % using Equation (1).[26]

$$\text{Bias}(\%)=\left(\frac{\text{Predicted}-\text{Actual}}{\text{Actual}}\right)\times 100 \quad (1)$$

Table 2 Experimental Runs for Optimization of Loratadine Loaded Zein Tannic Acid Nanoparticles and 5-Fluorouracil Loaded Zein Tannic Acid Nanoparticles

Run	X1: Zein Amount (mg)	X2: Tannic Acid (mg)	X3: Loratadine/5-Fluorouracil (mg)
1	62.5	125	6.25
2	100	125	2.5
3	100	200	6.25
4	100	50	6.25
5	100	125	10
6	62.5	200	10
7	25	125	2.5
8	62.5	125	6.25
9	62.5	125	6.25
10	25	200	6.25
11	25	125	10
12	62.5	125	6.25
13	62.5	200	2.5
14	62.5	50	10
15	62.5	50	2.5
16	25	50	6.25
17	62.5	125	6.25

Abbreviations: ZN, Zein; TAN, Tannic acid; LOR, Loratadine; FU, 5-Flourouracil.

Design Responses

The NPs size (nm), PDI, and ZP (mV) represented by Y1, Y2, and Y3, respectively, were assessed through dynamic light scattering technique (DLS) using Malvern Zeta sizer Nano ZS (Malvern Instruments, Malvern, UK). All samples were tested in triplicates at 25°C.

In addition, the EE% (Y4) of both LOR-ZN/TAN NPs and FU-ZN/TAN NPs formulations. Each formula was assessed individually through re-suspension in 3 mL of either deionized water or absolute ethanol and then left in a shaking incubator at 37°C for 72 h. This was performed to guarantee the complete extraction of the entire amount of incorporated drug. Afterward, the extracted drug was obtained via syringe filtration. The concentration of each of the two drugs (LOR or FU) was estimated individually using a UV-visible spectrophotometer (Evolution UV 600, Thermo Scientific, USA) at an absorbance of 275 nm and 265 nm, respectively. Finally, EE% was calculated using Equation (2).[28]

$$\%\text{Entrapment Effeciency} = \left(\frac{\text{Drug amount}}{\text{Theoretical drug amount}}\right) \times 100 \tag{2}$$

Morphological and Physicochemical Characterizations

Optimized formulations of both LOR-ZN/TAN and FU-ZN/TAN NPs were examined morphologically using transmission electron microscopy (TEM, Jeol, USA). A drop of each diluted nanosuspension of each developed nanoparticle was placed on a separate TEM copper grid and stained using phosphotungstic acid dye. Afterward, the NPs were investigated using TEM to determine their morphological features, in terms of shape and size.

Chemical analysis of both LOR-ZN/TAN and FU-ZN/TAN NPs was performed using Thermo Scientific Nicolet iS50 FTIR spectrometer (600–4000 cm^{-1}, 4 cm^{-1} resolution, 32 scans per spectrum). The study involved chemical structural analysis of free LOR, free 5-FU, and unloaded and loaded ZN/TAN NPs.

In-vitro Release Study

The release profiles of LOR and 5-FU from the corresponding optimized ZN/TAN NPs were investigated using the dialysis bag method. The nanosuspension of each of the LOR-ZN/TAN NPs and FU-ZN/TAN NPs (1 mL) was placed individually into a dialysis bag (Spectra Por 7,10 Kd) and inserted into a 50 mL falcon tube containing 30 mL of the abovementioned receptor medium. The release setup was maintained in a shaking incubator throughout the release study at 37 °C. At predetermined time points, a 1 mL aliquot of the release medium was withdrawn and replaced with fresh medium. The concentrations of released LOR and 5-FU were measured at wavelengths of 275 nm and 265 nm, respectively, using a UV-visible spectrophotometer. In addition, an equivalent amount of free LOR or 5-FU was also investigated for their release profile to compare the behavior of both drugs as free drugs and as incorporated drugs within the ZN/TAN NPs matrices. The cumulative release % was calculated using Equation (3) and plotted on the y-axis against time (h) on the x-axis. All samples were tested in triplicate.

$$Cn = Cn\,means + \mathrm{A/V}\sum_{s=1}^{n-1} Cs\,means \tag{3}$$

Where Cn represents the expected concentration of the nth sample, and Cn refers to the corresponding estimated concentration. A indicates the withdrawn aliquot volume from the receptor medium and V denotes the total volume of the dissolution medium. n−1 is the total sample volume that was withdrawn previously, whereas Cs represents the cumulative concentration of the aliquots collected before the currently measured sample.

The LOR and 5-FU release profiles were analyzed using various release kinetics models, including zero-order, first-order, Higuchi, Korsmeyer–Peppas, Hixson-Crowell, Hopfenberg and Baker-Lonsdale.[29]

In-vitro Cell Studies

Cytotoxicity Assessment

An in vitro cell study was performed to assess the cytotoxic activity of free LOR, free 5-FU, unloaded ZN/TAN NPs, LOR-ZN/TAN NPs, and FU-ZN/TAN NPs independently. The MCF-7 (HTB-22) human breast adenocarcinoma cell line (ATCC) was used for the cytotoxicity experiment under sterile conditions, where the cells were maintained in Dulbecco's

modified Eagle's medium (DMEM) supplemented with 100 µg/mL streptomycin, 100 U/mL penicillin, and 10% fetal bovine serum, and were cultured at the temperature of 37°C in a humidified atmosphere containing 5% CO_2 to ensure ideal viability.

A sulforhodamine B (SRB) assay was performed to measure cell viability. Briefly, 100 µL aliquots containing 5×10^3 cells were seeded into 96-well plates and incubated for 72 h. Afterward, the cells were treated with 100 µL fresh medium containing varying concentrations of one of the tested samples, each applied separately for 24 h. Afterward, the medium was replaced with 10% trichloroacetic acid (TCA, 150 µL) for cell fixation, then incubated for 1 h at 4°C. The TCA was discarded before washing the cells with deionized water (5x).

Subsequently, 0.4% (w/v) SRB solution (70 µL) was added, and the plates were incubated for 10 min at room temperature. The wells were washed with deionized water (3x) and left to dry in air. Next, 10 mM TRIS buffer (150 µL) was used to solubilize the protein-bound dye. Finally, the half-maximal inhibitory concentration (IC_{50}) was calculated using equation (4) for each sample by measuring the absorbance at 540 nm using a FLUOstar Omega microplate reader (BMG LABTECH, Ortenberg, Germany).[30]

$$\%\text{Viability} = \left(\frac{\text{Treated cells absorbance} - \text{Blank absorbance}}{\text{Control absorbance} - \text{Blank absorbance}}\right) \times 100\% \quad (4)$$

Apoptosis/Necrosis Assay

The proportion of cells undergoing apoptosis and necrosis after treatment with free LOR, free 5-FU, unloaded ZN/TAN NPs, LOR-ZN/TAN NPs, and FU-ZN/TAN NPs was estimated using the Annexin V-FITC Apoptosis Detection Kit (Abcam Inc., Cambridge Science Park, Cambridge, UK) and dual-channel flow cytometry (ACEA NovoCyte™, ACEA Biosciences Inc., San Diego, CA, USA). Cells treated for 24 h with the IC_{50} concentrations of each formulation were used in this analysis. Cells cultured in the medium alone without any treatment were also tested as a negative control.

Afterward, around 10^5 cells were collected through trypsinization, then washed with iced PBS, pH 7.4 (2x). Each treatment group was then dark incubated with Annexin V-FITC/propidium iodide (PI) staining solution (0.5 mL) in the dark for 30 min at 25°C. Finally, stained cells were assessed using a flow cytometer (ACEA Biosciences Inc., San Diego, CA, USA). Fluorescence was assessed using the FL1 and FL2 channels for FITC (λ_ex/em = 488/530 nm) and PI (λ_ex/em = 535/617 nm), respectively.

The extent of apoptosis, necrosis, and viable cells was determined by quantifying the populations in which FITC and/or PI staining was considered positive, as explained by Soule et al. Necrotic, apoptotic, viable (unstained), and early apoptotic cells were identified in quadrants Q1, Q2, Q3, and Q4, respectively.[5]

Cell Cycle Analysis

MCF-7 breast cancer cells were divided into six groups based on the administered treatment. The negative control group received no treatment, whereas the other five groups were treated with free 5-FU, unloaded ZN/TAN NPs, LOR-ZN/TAN NPs, FU-ZN/TAN NPs, or a combination of LOR-ZN/TAN NPs and FU-ZN/TAN NPs (1:1). The treated cells were incubated for 72 h, and cell cycle distribution was evaluated for each group.

Afterward, cells were harvested by trypsinization and washed with ice-cold PBS (pH 7.4 (2x)). Then, the collected cells were fixed by being resuspended in 60% cold ethanol (2 mL) before being incubated for 1 h at 4°C. After cell fixation, cells were washed again with PBS, PH 7.4 (2x) before in dark incubated at 37°C for 20 min with PBS (1 mL) containing 10 µg/mL propidium iodide (PI) and 50 µg/mL RNase A for staining in order to quantify cellular DNA content.

Finally, flow cytometry analysis was performed using the FL2 channel (λ_ex/em = 535/617 nm) with an ACEA NovoCyte™ flow cytometer. Data were collected from 12,000 cells for each sample, and the cell cycle phase distribution (G_0/G_1, S, and G_2/M) was determined using the ACEA NovoExpress™ software.[30]

Table 3 Docking Scores and Cavity Properties of Drug–Polymer Complexes

Drug	Polymer	Gibbs Free Energy (kcal/mol)	Cavity (A°)	Binding Center Coordinates (x, y, z)
Loratadine	Chitosan Zein	−6.7 **−8.5**	2476 1319	(−9, 21, 6) (−23, 20, −26)
5-Fluorouracil	Chitosan Zein	−4.9 **−5.5**	1319 2476	(−23, 20, −26) (−9, 21, 6)

Statistical Analysis

All quantitative data are presented as mean ± SD (n = 3). One-way analysis of variance (ANOVA) followed by Tukey's posthoc test was used to test the significance of the results obtained using GraphPad Prism Software version 6, where $*p < 0.05$, $**p < 0.01$, $***p < 0.001$, and $****p < 0.0001$.

Results

In-silico Studies

Binding Affinity Between Polymers and Drugs

The best binding affinities of each of the two drugs with each of the two polymers are listed in Table 3. This step was performed to determine the most suitable polymer for this study. The demonstrated results obtained for the binding energy scores confirmed that both LOR and 5-FU interacted more favorably with zein compared chitosan. This enhanced the entrapment efficiency of the loaded drugs within the designed polymeric nanocarrier system.[4]

Visualization of Zein Interactions with Drugs

BIOVIA Discovery Studio Visualizer (v19.1) software was used to visualize and investigate the interaction between zein on one side and LOR and 5-FU individually on the other side, as shown in Figure 1 and Table 4. Both Figure 1 and Table 4 show the interaction between zein and each of the two drugs, highlighting the amino acids, bonds, or interactions involved, as well as the calculated distance of the bonds.

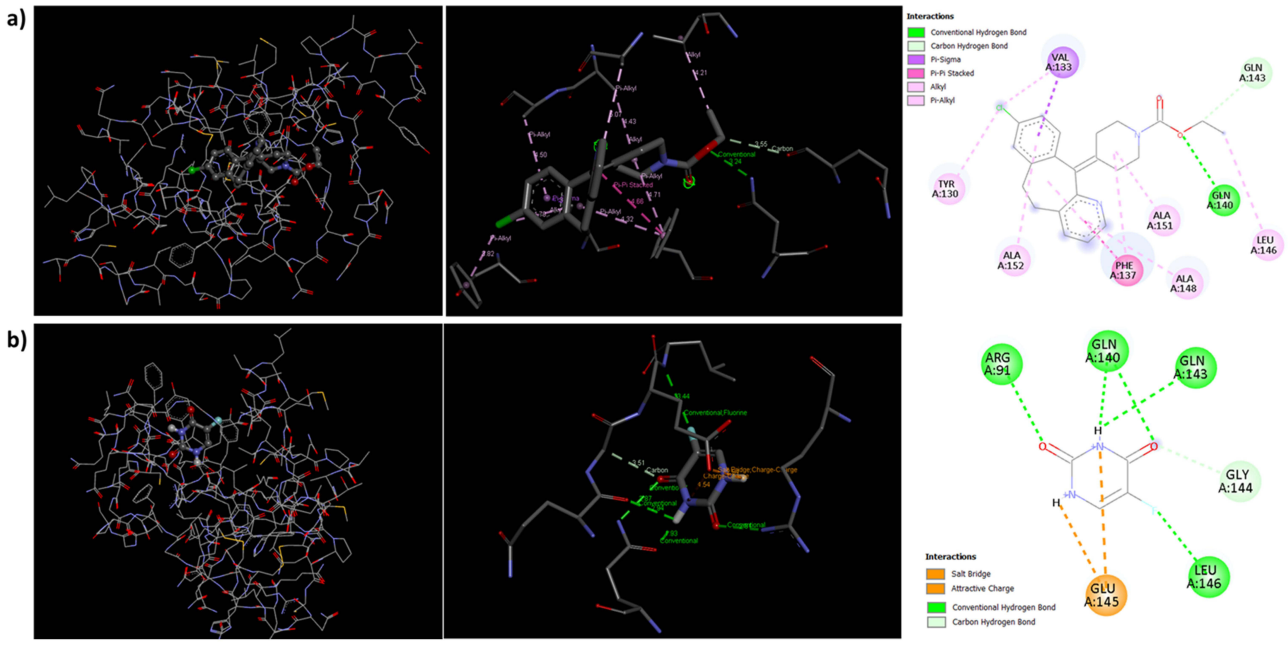

Figure 1 Overview of the molecular interaction, bond distance, and schematic 2D diagrams for molecular interaction between zein and (**a**) LOR and (**b**) 5-FU.

https://doi.org/10.2147/IJN.S564050

Table 4 A Summary of Types of Molecular Interactions Detected Between Zein and Either LOR or 5-FU Demonstrating the Involved Amino Acids, Types of Bonds or Interactions and Distances of Detected Bonds

Ligand	Residue	Type of Interaction	Distance (Å)
Loratadine	GLN A:140	Conventional Hydrogen Bond	3.24
	GLN A:143	Carbon Hydrogen Bond	3.44
	PHE A:137	π–π Stacked	5.78
	VAL A:133	π–Alkyl	4.50
	LEU A:146	π–Alkyl	4.32
	ALA A:151	π–Alkyl	4.66
	ALA A:152	Alkyl	4.82
5-Fluorouracil	GLU A:145	Salt Bridge (Electrostatic)	4.54
	ARG A:91	Conventional Hydrogen Bond	3.93
	GLN A:140	Conventional Hydrogen Bond	3.55
	GLN A:143	Conventional Hydrogen Bond	3.81
	LEU A:146	Carbon Hydrogen Bond	3.60
	GLY A:144	Carbon Hydrogen Bond	3.87

Zein-LOR Molecular Interactions

As shown in Figure 1a, LOR is incorporated within the hydrophobic cavity of the zein structure, resulting in a variety of stabilizing molecular interactions. For instance, π–π stacking occurred between the LOR aromatic ring and PHE:A137 within the zein structure. Furthermore, π–alkyl interactions were observed between each of the amino acid ALA:A151, VAL:A133, and LEU:A146 and LOR structures. In addition, GLN:A140 and GLN:A143 in zein form conventional hydrogen bonds with LOR. Finally, Carbon–hydrogen bonds were detected between the LOR and GLY:A144 in zein. These molecular interactions led to the successful formation of a stabilized polymer-drug network, predicting the sustained encapsulation of the drug.

Zein-5-FU Molecular Interactions

Figure 1b shows the molecular interactions between zein and 5-FU. It has been found also that 5-FU has a high binding affinity for zein, confirming the promising capability of zein as a polymeric nanocarrier to incorporate 5-FU efficiently. For instance, salt bridges and attractive charge interactions have been detected between 5-FU and amino acid GLU:A145 within the zein structure. Furthermore, conventional hydrogen bonding was observed between 5-FU and zein structures through the amino acids GLN:A140, ARG:A91, and LEU:A146. Moreover, fluorine-mediated hydrogen bonding interactions suggest the ability of zein to stabilize polar compounds. This can be attributed to the capability of the docking pocket to provide an appropriate electrostatic environment that retains the polar structure of 5-FU, confirming the versatility of zein as a dual-drug delivery system for both LOR and 5-FU.

Nanoparticles Development

Preliminary Screening

The effects of different variables used during preliminary screening for the preparation of FU-ZN/TAN NPs were evaluated on various attributes, including particle size, PDI, zeta potential (ZP), and entrapment efficiency (EE%), as shown in Table 5.

It can be inferred from Table 3 that applying homogenization and probe sonication during the preparation methods significantly enhanced both particle size and PDI. For instance, F1 exhibited the smallest nanoparticle size (387.9 nm) and narrowest PDI (0.345) while maintaining the highest EE% (90.6%). In contrast, the absence of homogenization and probe sonication resulted in the formation of a broader size distribution and a low EE%.

Furthermore, it was observed that increasing the volume of the aqueous phase (F3 and F4) resulted in an increase in both particle size and distribution. This can be attributed to the lack of efficient precipitation kinetics during preparation.

Table 5 Preliminary Screening for Formulation Conditions

F	Aq. Phase (mL)	H/S Applied	Size (nm)	PDI	ZP (mV)	EE (%)
F1	15	Yes	387.9	0.345	−21.9	90.6
F2	15	No	387.6	0.441	−25.1	68.7
F3	30	Yes	497.3	0.633	−24.7	67.6
F4	30	No	475.1	1.000	−21.1	71.7
F5	30	Yes	450.4	0.397	−22.4	83.2
F6	30	No	460.2	0.498	−23.2	77.3

Abbreviations: Aq, aqueous phase volume; H/S, Phase, and homogenization/sonication; PDI, Polydispersity index; ZP, Zeta Potential; EE, Entrapment Efficiency.

All tested formulations exhibited a surface charge (zeta potential) of −21 to −25 mV, indicating the formation of stabilized formulations with minimized aggregation probabilities.

Based on the results obtained from the preliminary screening, F1 was selected as the ideal formulation with the most promising conditions for further optimization using an experimental design. These preliminary findings aided in the selection of input variables for building the Box–Behnken experimental design to obtain the final optimized nanoparticle system.

Experimental Design

Analysis of Box-Behnken Design Output

Preparation of different LOR-ZN/TAN and FU-ZN/TAN NPs formulations was carried out based on the Box-Behnken design (BBD) built up using Design Expert software. The design suggested 17 experimental runs for each of the drug-loaded ZN/TAN NPs, as shown in Table 2, to investigate the influence of the various tested variables at different levels. It has been observed that all of the tested dependent variables were denoted by a quadratic model for both LOR-ZN/TAN NPs and FU-ZN/TAN NPs formulations as shown in Tables 6 and 7, respectively, except the PDI of FU-ZN/TAN NPs

Table 6 Analysis of BOX-BEHNKEN DESIGN Output Shows the Model of Loratadine Loaded Zein Tannic Acid Nanoparticles

Response	Model	R^2	Adjusted R^2	Predicted R^2	Adequate Precision	F-value	*p*-value
Size (Y1)	Quadratic	0.9347	0.8507	0.5095	10.7521	11.13	0.0022
PDI (Y2)	Quadratic	0.9853	0.9665	0.8559	17.7098	52.22	< 0.0001
Charge (Y3)	Quadratic	0.8800	0.7258	0.5889	7.6296	5.70	0.0159
EE (Y4)	Quadratic	0.9532	0.8931	0.9069	12.4324	15.86	0.0007

Table 7 Analysis of BOX-BEHNKEN DESIGN Output Showing the Model of 5-Fluorouracil Loaded Zein Tannic Acid Nanoparticles

Response	Model	R^2	Adjusted R^2	Predicted R^2	Adequate Precision	F-Value	*p* -value
Size (Y1)	Quadratic	0.9940	0.9862	0.9518	37.6939	128.04	< 0.0001
PDI (Y2)	Linear	0.5008	0.3856	0.1216	7.1934	4.35	0.0250
Charge (Y3)	Quadratic	0.9101	0.7946	0.2304	10.5754	7.88	0.0063
EE (Y4)	Quadratic	0.9752	0.9432	0.6323	18.0206	30.53	< 0.0001

https://doi.org/10.2147/IJN.S564050

which exhibited linear model. Furthermore, all adequate precision values exceeded four, suggesting that the following models of both drug-loaded formulations could be considered promising for fitting the experimental design space. Moreover, both the adjusted R2 and predicted R2 values were comparable, reflecting the reliability of the experimental design and suggested model. The influence of each of the tested factors on the evaluated responses was studied, and the results were plotted in 3D diagrams, as shown in Figures 2 and 3 for the LOR-ZN/TAN and FU-ZN/TAN NPs, respectively. The correlation coefficients are listed in Tables 8 and 9.

Particle Size

Particle size is a crucial factor to be considered during nanocarrier design because a smaller nanoparticle size results in a larger surface area, leading to the incorporation of larger amounts of bioactive cargoes.[31]

LOR-ZN/TAN NPs. LOR-ZN/TAN NPs size varied from 195.5 to 766.2 nm as demonstrated in Figure 2a–c. BBD statistical analysis demonstrated in Table 6 revealed that nanoparticle size exhibited a quadratic model (p = 0.0022) possessing an R^2 value of 0.9347 and adjusted R^2 value of 0.8507, confirming a reliable significant model fit of the experimental design.

Table 8 shows that both zein amount (X_1) and Loratadine concentration (X_3) significantly affect particle size exhibiting p = 0.0027 and p = 0.0238, respectively, along with regression coefficients of +22.92 and −7.44. Figure 2a–c also demonstrated that increasing zein amounts resulted in a proportional nanoparticle size increase. This can return back to the increased protein aggregation during nanoprecipitation, resulting in the formation of larger NPs. On the contrary, LOR exhibited a size-reducing effect. This may be attributed to the LOR hydrophobic nature, thus interacting with the hydrophobic cavities of ZN, enhancing molecular interaction and minimizing the nanoparticles hydrodynamic size.

In addition, the quadratic term X_3^2 (LOR^2) was highly significant ($p < 0.0001$), along with a large negative coefficient (−272.987), confirming the strong nonlinear suppressive effect of higher LOR concentrations on the nanoparticle size. The 3D response plots shown in Figure 2a–c confirm that formulations with higher LOR concentrations led to the formation of smaller NPs.

Tannic acid amounts (X_2) showed a negligible influence on particle size (p = 0.7584) compared to zein and LOR since it exhibited a coefficient of −105.63 indicating a negligible significance. These findings are in good agreement with the in silico data presented above, where LOR possessed a high binding affinity toward zein, resulting in a reduction in nanoparticle size.

FU-ZN/TAN NPs. The small size of the FU-ZN/TAN NPs was highly noticeable owing to the low molecular weight and hydrophilic nature of 5-FU, which easily diffuses during dissolution. The obtained nanoparticle sizes ranged from 147.3 to 404.8 nm as shown in Figure 3a–c. Statistical analysis demonstrated in Table 7 reveal that nanoparticle size followed a quadratic model ($p < 0.0001$) confirming a promising experimental design model with R^2 = 0.9940, adjusted R^2 = 0.9862, and predicted R^2 = 0.9518. Furthermore, the model exhibited an F-value of 128.04 confirming its reliability and significance.

Table 9 shows that nanoparticle size was significantly and proportionally influenced by both zein amount (X_1) (p = 0.0002, coefficient = +0.9976) and 5-FU concentration (X_3) (p = 0.0015, coefficient = +0.8303). Furthermore, the nonlinearilty of X_3^2 possessed high significance ($p < 0.0001$, coefficient = +5.30692), confirming the direct proportional increase in nanoparticle size at higher 5-FU concentrations.

In contrast, tannic acid amount (X_2) exhibited a moderate negative influence (p = 0.0001, coefficient = −1.94684), confirming that its crosslinking capability aided in the formation of more compact NPs with reduced size, as illustrated in Figure 3a–c. In addition, the X_1*X_2 term was statistically significant (p = 0.0116), confirming that the combined increase in both zein and tannic acid amounts significantly contributed to nanoparticle size minimization.

The response surface plots shown in Figure 3a–c clearly reveal that intermediate levels of zein and high-tannic acid result in the formation of smaller NPs.

Polydispersity Index

PDI is a critical parameter that indicates nanoparticle quality because it reflects the distribution uniformity of the

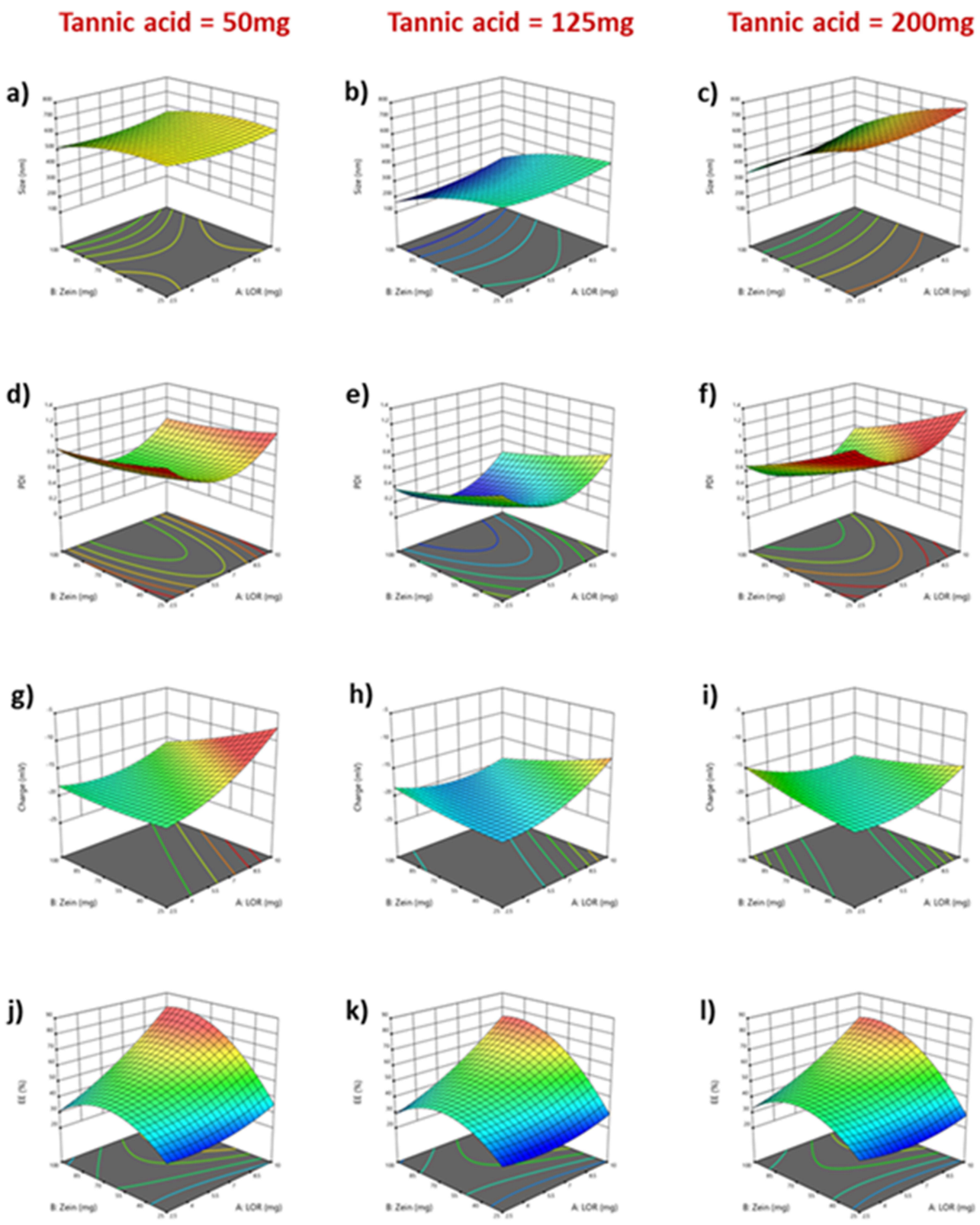

Figure 2 3D plots of evaluated responses for Loratadine Loaded Zein Tannic Acid Nanoparticles: (**a–c**) Size, (**d–f**) PDI, (**g–i**) ZP and (**j–l**) EE%.

https://doi.org/10.2147/IJN.S564050

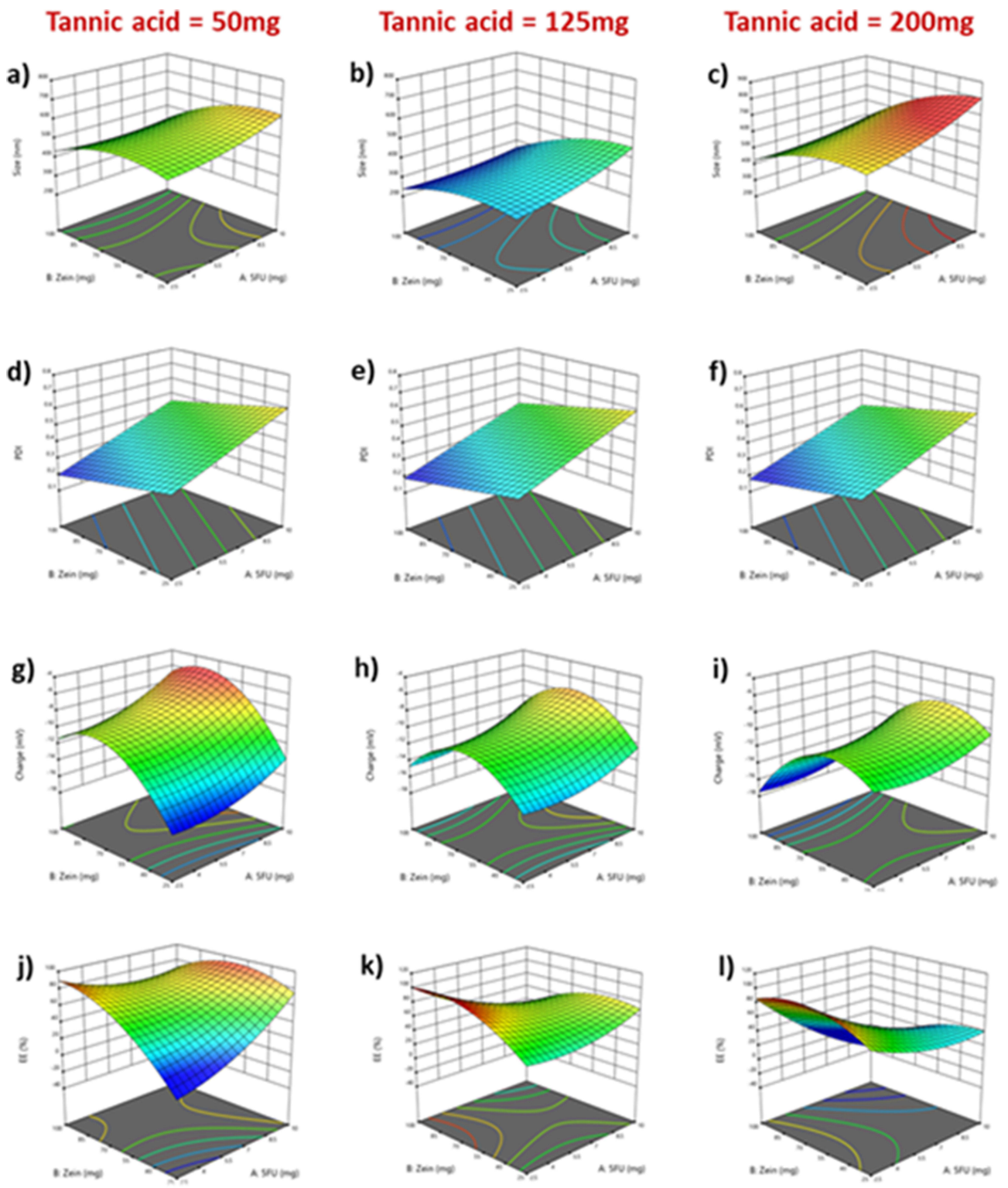

Figure 3 3D plots of evaluated responses for FU-ZN/TAN NPs: (**a–c**) Size, (**d–f**) PDI, (**g–i**) ZP and (**j–l**) EE%.

nanoparticle size within a formulation. PDI values range between 0 and 1, where monodisperse systems possessing high distribution uniformity exhibit values approaching 0, whereas those possessing high polydispersity exhibit values approaching 1.

Table 8 Regression Coefficients and Corresponding *p*-values Showing the Statistical Relationships Between the Investigated Formulation Factors and Their Respective Response Variables for Loratadine Loaded Zein Tannic Acid Nanoparticles

	Intercept	X1	X2	X3	X1*X2	X1*X3	X2*X3	X1²	X2²	X3²
Size	316.533	22.916	**−105.63**	−7.4458	11	13.5	−61.341	29.145	−39.012	**272.987**
***p*-values**		0.3577	**0.0027**	0.7584	0.7480	0.6940	0.1047	0.3939	0.2634	**< 0.0001**
PDI	0.218	0.0210	**−0.2033**	0.01528	0.0060	0.02	**−0.1064**	**0.3536**	0.0372	**0.408325**
***p*-values**		0.3552	**< 0.0001**	0.4962	0.8459	0.5280	**0.0096**	**< 0.0001**	0.2451	**< 0.0001**
Charge	−20.09	**1.6762**	−1.0275	−0.8537	**−2.0325**	−1.53	1.0175	**1.91**	0.4625	**1.995**
***p*-values**		**0.0122**	0.0789	0.1314	**0.0238**	0.0672	0.1933	**0.0276**	0.5236	**0.0231**
EE	49.842	**12.36**	**12.415**	−1.3475	**10.11**	−2.245	6.143E-16	4.854	**−15.651**	2.889
***p*-values**		**0.0003**	**0.0003**	0.4960	**0.0066**	0.4256	1.0000	0.1027	**0.0005**	0.3009

Notes: * *p* – value shading: $p < 0.05$ are significant and displayed in bold text, p-values $0.05 \leq p < 0.1$ are marginally significant and $p \geq 0.1$ are considered insignificant and displayed in normal text.

Table 9 Regression Coefficients and Corresponding *p*-values Showing the Statistical Relationships Between the Investigated Formulation Factors and Their Respective Response Variables for 5-Fluorouracil Loaded Zein Tannic Acid Nanoparticles

	Intercept	X1	X2	X3	X1*X2	X1*X3	X2*X3	X1²	X2²	X3²
Sqrt(Size + 0.50)	18.6489	**0.99769**	**−1.94684**	**0.8303**	**−0.65694**	0.3865	**−0.4962**	**0.5131**	**−1.4005**	**5.30692**
***p*-values**		**0.0002**	**< 0.0001**	**0.0005**	**0.0116**	0.0864	**0.0376**	**0.0299**	**0.0001**	**< 0.0001**
PDI	0.391412	**0.12768**	−0.07543	−0.0102						
***p*-values**		**0.0084**	0.0899	0.8072						
Charge	−10.2467	**1.55791**	0.4375	−0.7170	0.30002	−0.4725	**−2.8083**	1.2037	**−4.1904**	0.22875
***p*-values**		**0.0154**	0.4011	0.1864	0.6778	0.5168	**0.0048**	0.1176	**0.0004**	0.7445
EE	70.9425	**−11.6534**	3.23116	**−9.5397**	**−22.9886**	**−25.287**	**−17.47**	**12.173**	**−20.471**	**−13.0006**
***p*-values**		**0.0012**	0.1891	**0.0036**	**0.0002**	**< 0.0001**	**0.0008**	**0.0054**	**0.0003**	**0.0038**

Notes: * *p* – value shading: $p < 0.05$ are significant and displayed in bold text, p-values $0.05 \leq p < 0.1$ are marginally significant and $p \geq 0.1$ are considered insignificant and displayed in normal text.

LOR-ZN/TAN NPs. LOR-ZN/TAN formulations showed PDI values ranging from 0.141 to 1.00, showing that specific formulations exhibited a highly uniform nanoparticle size distribution, while others possessed high nanoparticle size variability, as illustrated in Figure 2d–f.

The analysis of variance results demonstrated that PDI followed a quadratic model with strong statistical significance ($p < 0.0001$), confirming an outstanding model fit with $R^2 = 0.9853$ and adjusted $R^2 = 0.9665$. Furthermore, Table 8 shows that both zein (X_1) and LOR (X_3) significantly influenced the PDI, with *p*-values <0.0001 and 0.0096, respectively. It was also noticed that both variables had a negative effect on PDI because they recorded coefficient values of −0.2033 (X_1) and −0.1064 (X_3^2), confirming that increasing either zein or oratadine amounts resulted in improved homogeneity of the nanoparticle size distribution.

Figure 2d–f plots confirmed that the lowest PDI values were observed in formulations with higher Loratadine amounts and intermediate Zein amounts. This may be attributed to the intermolecular interactions between LOR and the hydrophobic Zein domains that enhance tighter molecular compaction and consequently reduce nanoparticle size variability. This is found to be in a good accordance with the in-silico results that showed strong binding affinity between LOR and zein through hydrophobic, π-stacking, and hydrogen bonding interactions.

In contrast, the tannic acid amount (X_2) possessed no significant influence on PDI ($p = 0.4962$), exhibiting a very low regression coefficient value of 0.01528. These results confirm that zein and LOR are the main influencers of PDI NPs.

FU-ZN/TAN NPs. As shown in Figure 3d–f that FU-ZN/TAN NPs possess PDI values of the FU-ZN/TAN NPs ranged from 0.141 to 0.841. This suggests that most of the prepared nanoformulations fell within an acceptable PDI range, where certain tested formulations approached monodispersity.

Unlike the LOR-ZN/TAN NPs, the PDI regression model for the FU-ZN/TAN NPs showed a linear fit, as shown in Table 7, where $R^2 = 0.5008$ and adjusted $R^2 = 0.3856$, illustrating a moderate predictive value for the selected model.

https://doi.org/10.2147/IJN.S564050

Among the investigated factors, only the zein amount (X_1) significantly influenced the PDI ($p = 0.0084$) value through an inverse relationship possessing a negative regression coefficient (−0.12768), as shown in Table 9. This may be attributed to the enhanced stability of zein polymeric matrices.

In contrast, Figure 3d–f illustrated that neither tannic acid (X_2) nor 5-FU (X_3) had a statistically significant effect on the PDI ($p > 0.05$). It has been also found that lower PDI values were noticed in formulations possessing higher zein while lower 5-FU amounts, highlighting the role of polymer–drug interaction in formation of NPs with narrow PDI values.

Hence, it was concluded that the amount of zein was the chief driving factor for PDI improvement in both the drug-loaded formulations.

Surface Charge

The surface charge or zeta potential (ZP) is a crucial attribute that determines the stability of nanoparticulate systems. NPs possessing either high positive or negative ZP values show high stability due to increased electrostatic repulsion, which prevents aggregation and consequently sedimentation.[31–33]

LOR-ZN/TAN NPs. It has been observed that LOR-ZN/TAN NPs formulations possess ZP values range from −12.06 to −22.27 mV, highlighting moderate to high NPs stability as shown in Figure 2g–i. Table 6 illustrates an acceptable model fit design ($p = 0.0159$) followed a quadratic regression possessing $R^2 = 0.8800$ and adjusted $R^2 = 0.7258$.

Table 8 illustrates that zein amount (X_1) was the only variable that exhibits a statistically significant influence on ZP ($p = 0.0122$), showing a positive coefficient of +1.6762. This suggests that increasing the amount of zein increased the surface charge of the NPs. This may be due to the abundance of ionizable carboxylic and amide groups within the zein structure, which became more noticeable at higher polymer concentrations, thus improving the surface charge density of the developed NPs.

Both tannic Acid (X_2) and LOR (X_3) amounts were found to show no statistical significance on ZP where the p-values recorded $p = 0.0789$ and 0.1314, respectively, as inferred from Table 8 and Figure 2g–i.

These results highlight that zein played the main role in increasing the surface charge of the developed formulations; however, both LOR and tannic had limited effects on ZP within the tested formulations.

FU-ZN/TAN NPs. FU-ZN/TAN NPs exhibited a broader range of ZP where it recorded a range from −6.82 to −27.85 mV as shown in Figure 3g–i. Results demonstrated in Table 7 confirmed that the ZP followed a quadratic model ($p = 0.0063$), possessing strong regression parameters with $R^2 = 0.9101$, and adjusted $R^2 = 0.7946$, confirming the suitability of the designed model.

Furthermore, Table 9 results reveal that both zein amount (X_1) ($p = 0.0154$, coefficient = +1.55791) as well as tannic acid amount (X_2) ($p = 0.0411$, coefficient = +0.97403) exhibit a significant direct proportional relationship with the ZP. This revealed that an increase in either zein or tannic acid content would consequently result in an increase in the net negative surface charge of the nanoformulations. This can be attributed to the abundance of phenolic and carboxylic groups in tannic acid and zein structures, respectively. This returns their ability to dissociate under neutral pH conditions, enhancing nanoparticle repulsion and, consequently, their stability.

Finally, Figure 3g–i confirm that the highest ZP values were obtained at high levels of both zein and tannic acid, with moderate 5-FU content. These results highlight the crucial role of both the polymer and crosslinker amounts in tailoring the surface charges on the developed NPs to enhance their stability.

Entrapment Efficiency

Entrapment efficiency is an important variable to investigate because it reflects the extent to which the drug is successfully incorporated into the polymeric matrix of the developed NPs formulations. A higher EE% allows for minimized efficient doses while improving drug delivery efficiency.

LOR-ZN/TAN NPs. The LOR-ZN/TAN formulations exhibited EE values ranging from 23.6% to 74.7%, as illustrated in Figure 2j–l. It was also observed that all three tested factors significantly influenced the EE% values, where zein (X1), tannic acid (X2), and LOR (X3) had p-values of 0.0003, 0.0003, and 0.0066, respectively (Table 8). Moreover, EE% was directly proportional to both zein and tannic acid amounts but inversely proportional to the amount of LOR. This was

confirmed by the zein, tannic acid, and LOR coefficient values, which were +12.36, +12.415, and −1.3475, respectively. Hence, the order of influence of EE% is Zein > TAN > LOR.

FU-ZN/TAN NPs. FU-ZN/TAN formulations showed EE% values ranging from 33.7% to 80.6%, as shown in Figure 3j–l. Similar to LOR-ZN/TAN NPs, Table 9 demonstrates that all three tested independent variables had a significant influence on EE%, with *p*-values of 0.0012, 0.0001, and 0.0003 for zein, tannic acid, and 5-FU, respectively. Unlike LOR-ZN/TAN NPs, EE% was inversely proportional to all three tested variables, with coefficients of −11.6534, −2.3116, and −9.5397 for zein, tannic acid, and 5-FU, respectively. Hence, the descending order of the influence of the variables on EE% was Zein > 5-FU > TAN.

Although molecular docking studies showed a stronger theoretical binding affinity between zein and LOR (ΔG = −8.5 kcal/mol) compared to 5-FU (ΔG = −5.5 kcal/mol), the EE% determined experimentally proved an opposite trend, where EE% of 5-FU (74.9%) recorded higher values compared to LOR (61.3%). This could be attributed to the physicochemical interactions and kinetics occurring during the assembly of drug loaded nanoparticles. For instance, LOR hydrophobicity limits its homogeneous partitioning within the aqueous and the alcoholic parts of the hydroalcoholic solvent system, resulting in reduced EE%, despite its high binding affinity. On the contrary, 5-FU's due to its higher hydrophilicity allows higher encapsulation within the tannic-acid-crosslinked zein matrices, leading to higher experimental EE% values.

Optimization

LOR-ZN/TAN NPs. Both numerical and graphical optimizations were carried out to determine the optimum formulation with the minimum nanoparticle size and PDI, as well as ZP and EE%. Both the desirability plot shown in Figure 4a and graphical overlay plot illustrated in Figure 4b reveal similar results, confirming the reliability of the proposed experimental design model. Design Expert® software proposed 30 possible solutions ranked in descending order based on overall desirability. The optimal formulation had a desirability value of 0.865. The suggested formulations were composed of X_1, zein (100 mg); X_2, tannic acid (131.9 mg); and X_3, LOR (8.24 mg). In addition, the software predicted that this formula would possess a nanoparticle size of 194.7 nm, PDI of 0.162, ZP of −20.35 mV, and EE% of 59.66%. Hence, the proposed formulation was prepared and re-characterized experimentally to validate the accuracy of the prediction proposed by the BBD.

FU-ZN/TAN NPs. FU-ZN/TAN formulations were optimized to obtain NPs with a minimized size and PDI, while maximizing ZP and EE%. 4c (desirability plot) and Figure 4d (overlay plot) show the numerical and graphical analyses, respectively, confirming the same results with a desirability score of 0.782. The optimal formulation was composed of X_1: zein (95.96 mg), X_2: tannic acid (131.9 mg), and X_3:5-FU (6.73 mg). According to the prediction obtained from BBD, this formula is expected to have a particle size of 213.89 nm, PDI of 0.154, ZP of −26.21 mV, and EE% of 72.67%. The selected formulation was reprepared and reanalyzed experimentally to confirm the accuracy of the proposed model.

Validation

The optimum formulations predicted by BBD for both drug-loaded NPs were prepared according to the aforementioned procedures. The size, PDI, ZP, and EE% of the obtained NPs were analyzed. Afterward, the obtained results for both LOR-ZN/TAN NPs and FU-ZN/TAN NPs were illustrated as actual values and compared with the predicted values obtained from the BBD, as shown in Tables 10 and 11, respectively. The observed values obtained from the characterization of both the optimized formulations were in good agreement with the predicted values. This suggests the high reliability of the BBD design generated by Drug Expert software.

Morphological and Chemical Characterizations

The morphology of the optimized formulations of both LOR-ZN/TAN and FU-ZN/TAN NPs was examined using TEM, as illustrated in Figure 5a and d, respectively. TEM images revealed that both NPs were successfully developed, and both formulations exhibited an almost spherical morphology. However, they were smaller than those of the DLS measure-

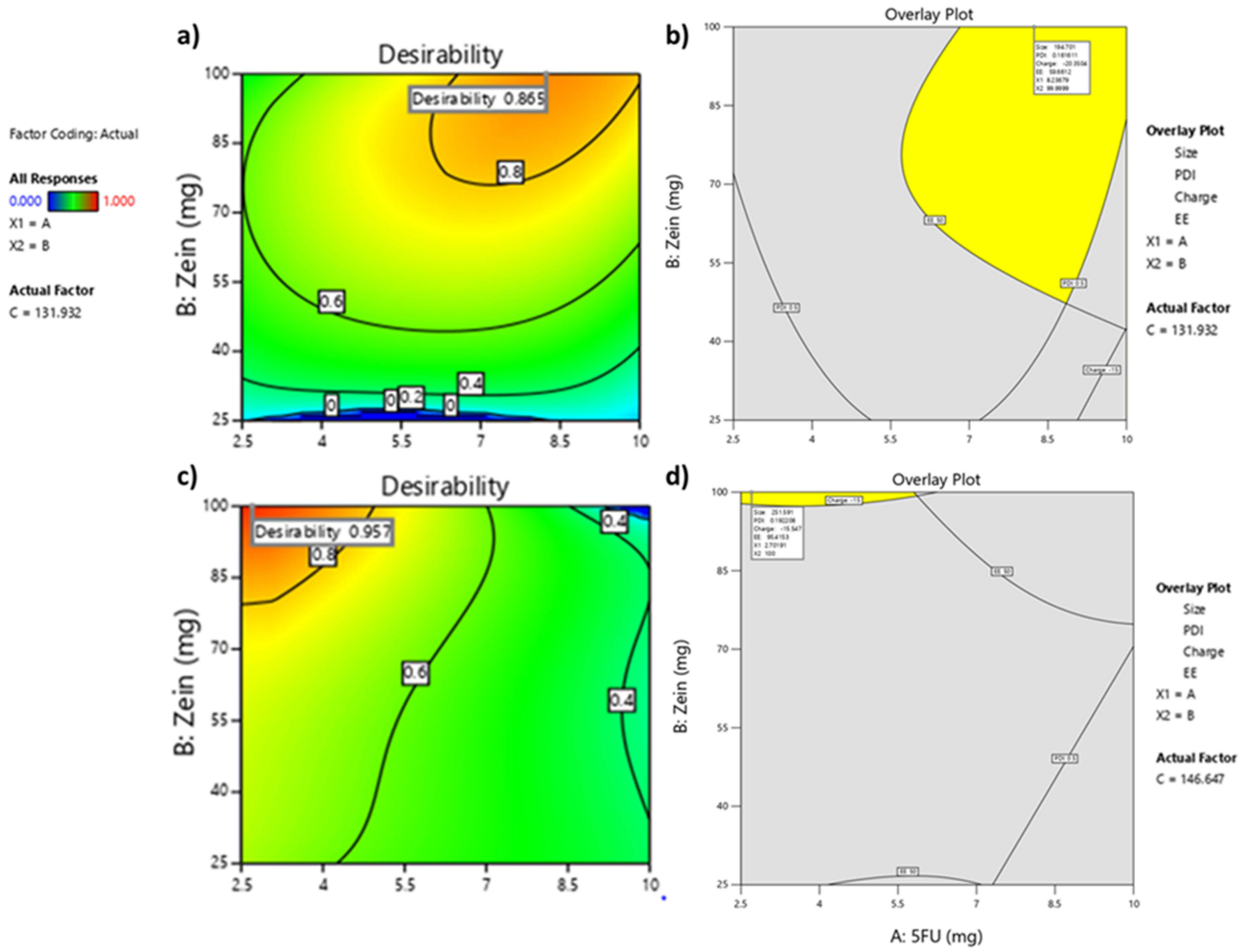

Figure 4 Optimization of the design factors: (**a**) desirability plot obtained from numerical optimization, (**b**) overlay plot obtained from graphical optimization of Loratadine Loaded Zein Tannic Acid Nanoparticles, (**c**) desirability plot obtained from numerical optimization, and (**d**) overlay plot obtained from graphical optimization of of FU-ZN/TAN NPs.

ments. This was attributed to the difference between the hydrodynamic size of the polymer-based nanocarriers obtained from DLS measurements and the size obtained from TEM imaging of dried samples. This is in good agreement with the results of previous studies.[34,35]

Table 10 The Observed and Predicted Values of Different Responses for the Optimized Loratadine Loaded Zein Tannic Acid Nanoparticles Formula

Response	Y1: Size (nm)	Y2: PDI	Y3: ZP (mV)	Y4: EE%
Actual Values	197.2	0.153	−21.78	61.33
Predicted Values	194.7	0.162	−20.35	59.66
Bias %	1.268	5.882	6.566	2.723

Table 11 The Observed and Predicted Values of Different Responses for the Optimized 5-Fluorouracil Loaded Zein Tannic Acid Nanoparticles Formula

Response	Y1: Size (nm)	Y2: PDI	Y3: ZP (mV)	Y4: EE%
Actual Values	231.22	0.170	−24.01	74.91
Predicted Values	213.89	0.154	−26.21	72.67
Bias %	7.473	9.412	9.163	2.990

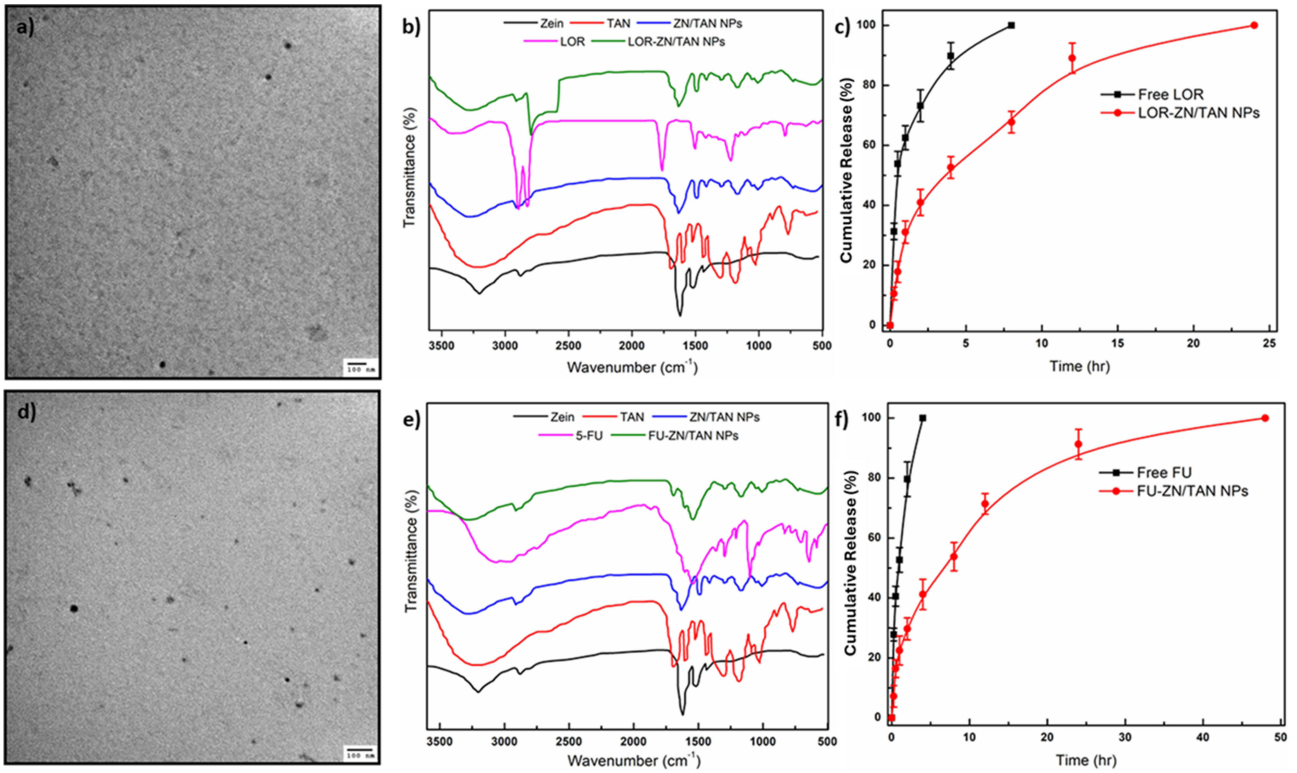

Figure 5 Characterization of Loratadine Loaded Zein Tannic Acid Nanoparticles and FU-ZN/TAN NPs: (**a** and **d**) TEM images of the optimum formulations, (**b** and **e**) FTIR Spectrum of their chemical structures and, (**c** and **f**) Cumulative release of free and incorporated drugs from their corresponding formulations.

Figure 5b shows the FTIR spectra of the zein, TAN, free LOR, ZN/TAN NPs, and LOR-ZN/TAN NPs. The zein FTIR spectrum revealed a characteristic band at 3200 cm^{-1}, attributed to N–H and O–H stretching vibrations, which are abundant in protein-based chemical structures. In addition, two distinctive peaks appearing at ~1650 cm^{-1} due to C=O stretching and ~1550 cm^{-1} due to N–H bending correspond to typical amides I and II, respectively, which are considered key bands for the zein protein backbone structure.[36]

The FTIR spectrum of TAN exhibited a distinct broad peak at ~3395 cm^{-1} and a sharp peak at ~1713 cm^{-1} due to O–H stretching and C=O stretching of the carboxylic acid groups. Additionally, the phenolic groups of TAN were detected by observing peaks at ~1611 cm^{-1} and 1532 cm^{-1} attributed to aromatic C=C stretching.[4]

The FTIR spectrum of LOR showed characteristic peaks at ~1600 cm^{-1} and ~1700 cm^{-1} contributed to the C=N stretching of the pyridine ring and C=O of the ester groups, respectively. The presence of a strong forked peak in the range 2750–2850 cm^{-1} is attributed to the C – H stretching of aromatic and heterocyclic rings within the LOR structures.[4]

ZN/TAN NPs successful formation is confirmed by the detection of a broad band at ~3400 cm^{-1}, which corresponds to the interaction between the O and H of TAN and the N–H of Zein. The appearance of a characteristic peak of LOR in the range of 2750–2850 cm^{-1} suggests its successful encapsulation within the ZN/TAN NPs.

Figure 5d shows the FTIR spectra of the zein, TAN, 5-FU, ZN/TAN, and FU-ZN/TAN NPs. The FTIR spectrum of FU showed several sharp peaks in the range 1300–1700 cm^{-1}, corresponding to both C–F and C=O and stretching vibrations, as well as the pyrimidine ring.[37] The FTIR spectrum of the FU-ZN/TAN NPs demonstrated the characteristic peaks of zein and TAN, as well as their interactions, similar to those of the LOR-loaded system. Furthermore, the appearance of the characteristic peaks of FU in the range 1300–1700 cm^{-1} was also detected with reduced intensity within the spectrum of FU-ZN/TAN NPs, confirming the successful incorporation of FU into FU-ZN/TAN NPs matrices.

https://doi.org/10.2147/IJN.S564050

In-vitro Release Study

The cumulative release of both LOR and 5-FU, either in their free or incorporated forms, was demonstrated as a plot of cumulative concentration % versus time in hours, as shown in Figure 5c and f, respectively.

Figure 5c shows that free LOR demonstrated a rapid release pattern, with complete release achieved within 8 h. In contrast, LOR-ZN/TAN NPs exhibited a significant sustained-release profile, extending up to 24-hour duration. An initial burst release phase of approximately 30% was detected within the first hour, followed by a sustained and controlled release phase owing to the diffusion pattern within the ZN/TAN NPs matrices. Furthermore, kinetic analysis revealed that LOR release from LOR-ZN/TAN NPs followed the Korsmeyer–Peppas model as the best-fitting model, with an r^2 value of 0.991, reflecting the diffusion mechanism of LOR from ZN/TAN NPs matrices.

In addition, the recorded dissolution efficiency (DE) values were 90.56% and 71.25% for free LOR and incorporated LOR from the LOR-ZN/TAN NPs, respectively, validating the prolonged LOR release behavior of the developed system. In addition, the mean dissolution time (MDT) increased from 1 hour to 4.34 hours when comparing free LOR to LOR-ZN/TAN NPs, again confirming the prolonged release pattern of the developed polymeric matrix.

Similarly, 5-FU, as a free drug, showed rapid release behavior and was completely released within 6 h. However, FU release from the FU-ZN/TAN NPs showed an extended pattern for up to 48 h. Furthermore, FU-loaded NPs also demonstrated an initial burst release of approximately 22% within the first hour, followed by a controlled and sustained release along 48-hour period.

Similar to LOR-ZN/TAN NPs, FU-ZN/TAN NPs followed the Korsmeyer–Peppas model as the best-fitting model, with an r^2 value of 0.981, reflecting the diffusion of 5-FU in the polymer-based matrices. The observed DE values for free FU and FU-ZN/TAN NPs were 96.15% and 78.11%, respectively, whereas MDT increased from 1.4 hours up to 6.5 hours when comparing free 5-FU to FU-loaded NPs.

The obtained release data was found to best fit with Korsmeyer–Peppas model. This indicates a non-Fickian diffusion, as the drug release is controlled through a mechanism combining diffusion from the hydrated polymeric matrices and relaxation of polymeric networks rather than standalone erosion only.

Although the release results demonstrate that free 5-FU exhibits a more rapid release profile compared to LOR, it showed a more sustained release from ZN/TAN NPs compared to LOR. These findings are in good agreement with the results obtained from in silico studies as well as entrapment experiments, which proved that 5-FU possesses a higher binding affinity to zein matrices, delaying their release.

In-vitro Cell Studies

Cytotoxicity Assessment

The cytotoxicity of free LOR, free 5-FU, ZN/TAN NPs, LOR-ZN/TAN NPs, FU-ZN/TAN NPs, and a 1:1 mixture of LOR-ZN/TAN and FU-ZN/TAN NPs was investigated by SRB assay using MCF-7 breast cancer cells. Varying concentrations (0.01–100 µg/mL) of each formulation were tested independently for 72 h, afterward which the cell viability was calculated.

The IC_{50} results analysis showed that FU-ZN/TAN NPs possess the highest cytotoxicity with an IC_{50} value of around 18 µg/mL, followed by free 5-FU at 25 µg/mL and ZN/TAN NPs at 30 µg/mL. On the other hand, free LOR and LOR-ZN/TAN NPs showed higher IC_{50} values of around 45 µg/mL and 50 µg/mL, respectively. Finally, the 1:1 mixture of LOR-ZN/TAN and FU-ZN/TAN NPs revealed an IC_{50} of approximately 40 µg/mL.

Figure 6a confirms that all tested formulations exhibited dose-dependent cytotoxicity, where a reduction in cell viability was observed with an increase in dose concentration. It was also observed that FU-ZN/TAN NPs exhibited the highest cytotoxicity among all tested formulations, resulting in the lowest cell viability %, followed by free 5-FU. In contrast, both free LOR and LOR-ZN/TAN NPs exhibited moderate cytotoxicity.

Interestingly, LOR-ZN/TAN NPs showed a slightly lower reduction in cell viability than the equivalent dose of free LOR, confirming that the incorporation of LOR within the ZN/TAN matrices resulted in delayed and sustained drug release.

Furthermore, the results showed that the cytotoxic effect of the mixed formulation of LOR-ZN/TAN and FU-ZN/TAN NPs (1:1) was similar to that of FU-ZN/TAN NPs alone, despite containing only half the FU dose. This is also supported by the IC50 values shown in Figure 6b. These results highlight the potential synergistic effect of LOR and FU when combined in a drug delivery system, allowing for a potential reduction in the required dose of 5-FU. Hence, this can be

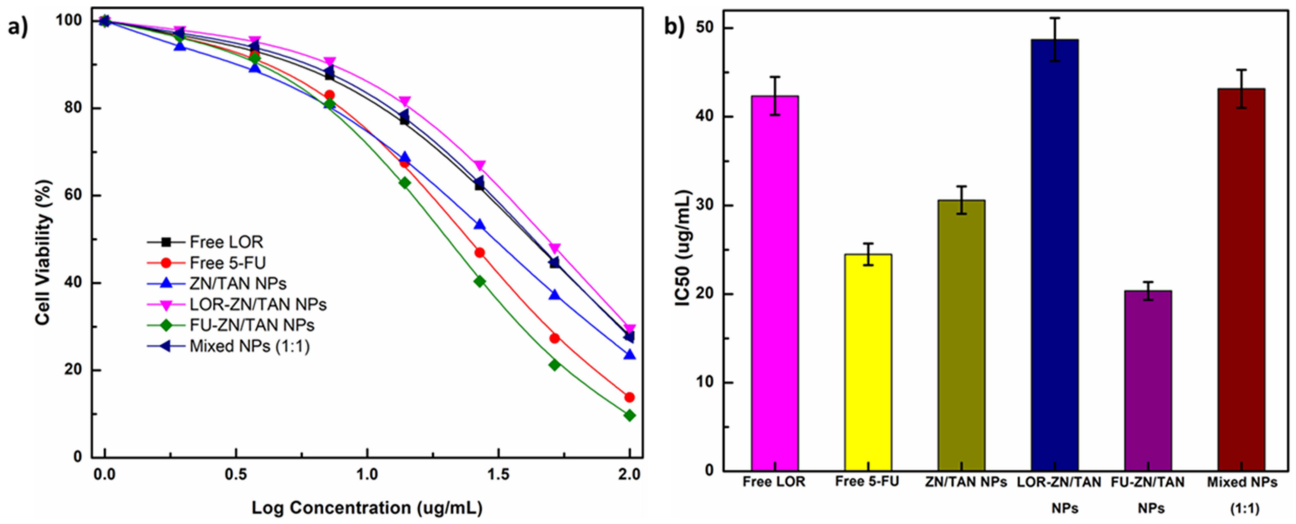

Figure 6 In-vitro cytotoxicity cell study: (**a**) Cell viability percentage and (**b**) IC_{50} of free LOR, free 5-FU, ZN/TAN NPs, Loratadine Loaded Zein Tannic Acid Nanoparticles, and FU-ZN/TAN NPs.

considered as a promising approach to may reduce 5-FU treatment associated systemic toxicity, introducing a more efficient and safer alternative for breast cancer therapy.

Annexin V/Propidium Iodide Apoptosis/Necrosis Assay

Results obtained from the apoptotic and necrotic effects of various treatments (free 5-Fluorouracil (5-FU), ZN/TAN NPs, LOR-ZN/TAN NPs, FU-ZN/TAN NPs, and a 1:1 mixture of LOR-ZN/TAN and FU-ZN/TAN NPs) on MCF-7 breast cancer cells are shown in Figures 7a–e. The study analysis highlights the proportion of cells undergoing necrosis (Q1),

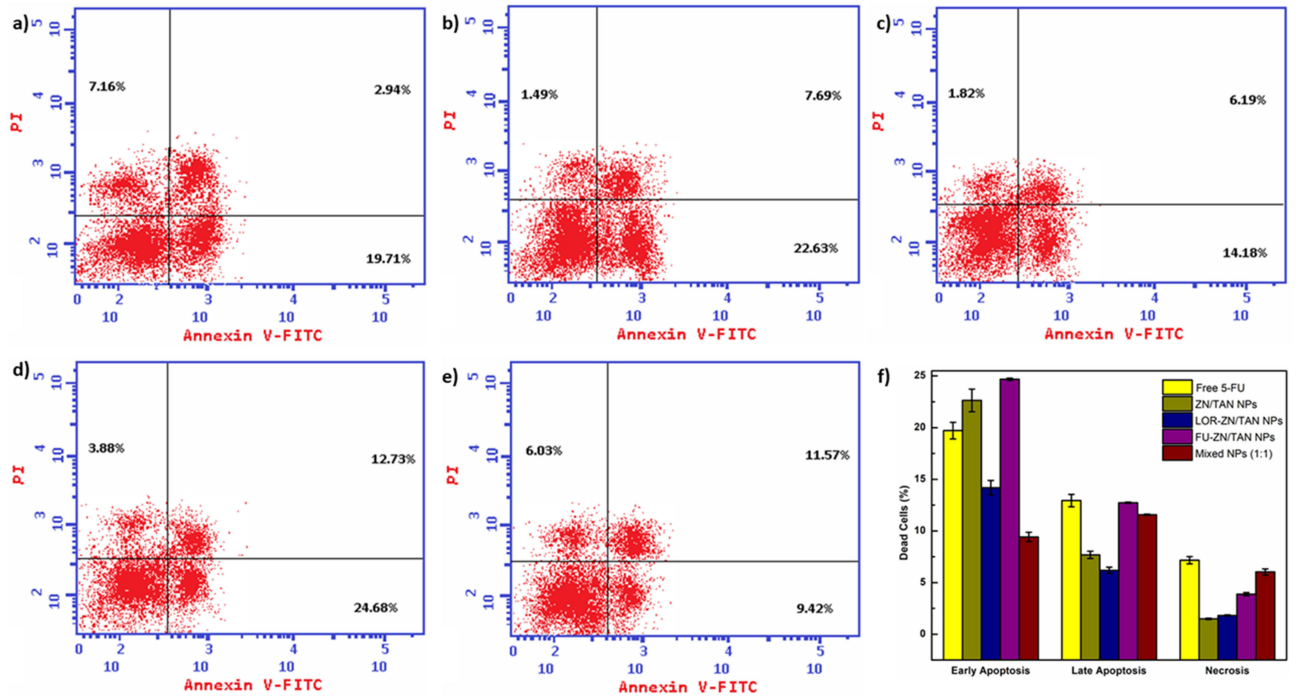

Figure 7 Annexin V/Propidium iodide apoptotic/necrotic assay analyzed by flow cytometry for breast cancer cells incubated with (**a**) free 5-FU, (**b**) ZN/TAN NPs, (**c**) Loratadine Loaded Zein Tannic Acid Nanoparticles, (**d**) FU-ZN/TAN NPs, (**e**) Mixed NPs (1:1), and (**f**) percentage of cells death of early apoptosis, late apoptosis, and necrosis for the different treatments.

https://doi.org/10.2147/IJN.S564050

late apoptosis (Q2), viability (Q3), and early apoptosis (Q4) after a 12-hour incubation with each treatment. The test groups were compared with untreated cells and free LOR, as discussed in a previous study.[4]

Furthermore, Figure 7f demonstrated that all treatment groups showed enhanced apoptosis compared with the controls. Notably, FU-ZN/TAN NPs possessed the highest potent apoptotic activity, showing 24.68% and 12.73% early and late apoptosis, respectively, confirming their high ability to stimulate programmed cell death. Similarly, free 5-FU showed a combined apoptotic index of 32.65% (early + late) and necrotic index of 7.16%, suggesting a moderate apoptotic level with a mixed mode of cell death.

In contrast, unloaded ZN/TAN NPs stimulated relatively less apoptosis, confirming their reduced therapeutic cytotoxicity as nanocarrier systems. LOR-ZN/TAN NPs also exhibited a moderate apoptotic effect compared to 5-FU loaded NPs and enhanced apoptotic activity compared to unloaded NPs.

Interestingly, the combination of LOR-ZN/TAN and FU-ZN/TAN NPs (1:1) induced a robust apoptotic response, approaching that of FU-ZN/TAN NPs, with early and late apoptosis levels of 9.42% and 11.57%, respectively. These results illustrate the strong apoptotic efficacy of the combined drug-loaded NPs.

These findings highlight the additive advantage of combining 5-FU- and LOR-loaded ZN/TAN NPs systems to enhance apoptosis rather than necrosis in MCF-7 breast cancer cells.

Cell Cycle Analysis

The influence of the tested treatments on cell cycle analysis in MCF-7 breast cancer cells was determined by flow cytometry after propidium iodide nuclear staining. The distribution of breast cancer cells was evaluated in different phases: G0-G1 (apoptotic or non-dividing cells), S phase (DNA synthesis phase), and G2-M phase (mitosis/proliferation). The results of the cell cycle analysis for free 5-FU, ZN/TAN NPs, LOR-ZN/TAN NPs, FU-ZN/TAN NPs, and a 1:1 mixture of LOR-ZN/TAN and FU-ZN/TAN NPs treatments are shown in Figure 8a–e. The results were compared with those of previously reported controls (untreated cells and free LOR).[4]

Figure 8f illustrates that treatment with free 5-FU resulted in a significant accumulation of cells in the S phase, suggesting blockage of DNA replication. It has been observed that around 48.25% of the cells were arrested in the S phase, which is found to be in a good accordance with the reported 5-FU mechanism as an antimetabolite in disrupting

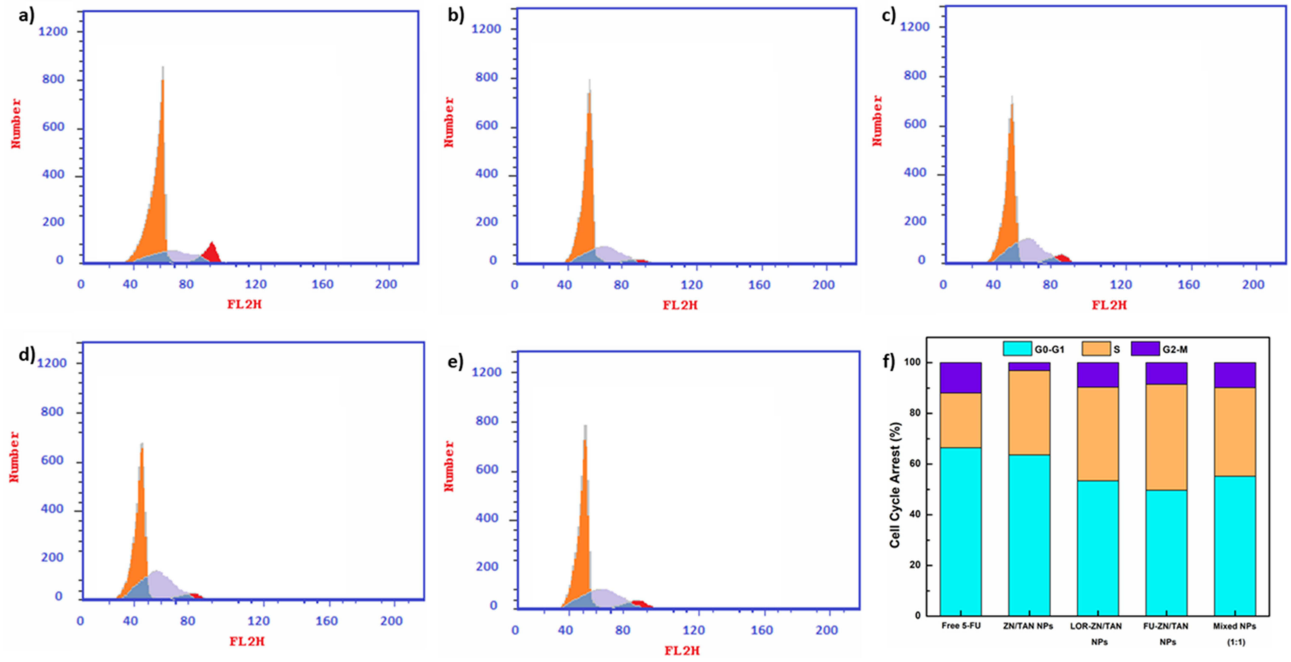

Figure 8 Cell cycle analyzed by flow cytometry for breast cancer cells incubated with (**a**) free 5-FU, (**b**) ZN/TAN NPs, (**c**) Loratadine Loaded Zein Tannic Acid Nanoparticles, (**d**) FU-ZN/TAN NPs, (**e**) Mixed NPs (1:1), and (**f**) percentage of cells cycle analysis.

DNA synthesis.[38] By contrast, the G0-G1 (30.71%) and G2-M (21.04%) phases exhibited moderate and minimal accumulation, respectively.

In contrast, ZN/TAN NPs induced a different pattern, where accumulation of the majority of cells (56.85%) was observed in the G0-G1 phase, followed by 28.71% in the S phase, and finally 14.44% in the G2-M phase. These results suggest that unloaded ZN/TAN NPs mainly induced cell cycle suppression in the non-dividing apoptotic phase without any significant interference with mitosis or DNA synthesis.

Similarly, LOR-ZN/TAN NPs showed a G0-G1 phase with the highest accumulation percentage (54.23%), with mild cells progressing in the S phase (29.55%) and the lowest accumulation in the G2-M phase (16.22%), validating the added effect of LOR on TAN to stimulate cell cycle arrest at the initial stages of cell division.

In contrast, FU-ZN/TAN NPs exhibited a remarkable increase in S phase accumulation, reaching 50.87%, which was higher than that of free 5-FU, accompanied by mild cell progression in G0-G1 (29.32%) and G2-M (19.81%) phases. This confirmed that the ZN/TAN NPs delivery system with FU significantly promoted its ability to halt cancer cells during DNA replication.

Interestingly, the mixture of LOR-ZN/TAN and FU-ZN/TAN NPs (1:1) showed intermediate behavior when compared to the individual drug-loaded NPs, where cell accumulation distributions in the G0-G1, S, and G2-M phases were 45.74%, 36.29%, and 17.97%, respectively. This suggests that the combination of LOR-ZN/TAN and FU-ZN/TAN NPs presents a new drug delivery system possessing a dual mechanism that targets both early cell cycle arrest and inhibition of DNA synthesis. Hence, the mixed formulation introduced a new balanced approach, exhibiting a significant inhibitory influence on multiple phases of the cell cycle, confirming its potential as a synergistic therapeutic agent for breast cancer management.

Discussion

In silico studies have proven that zein possesses superior binding affinity for both LOR and 5-FU compared to chitosan, where Gibbs free energy recorded −8.5 kcal/mol for zein-LOR complex compared to –6.7 kcal/mol for chitosan-LOR complex, and –5.5 kcal/mol for zein-5 FU complex compared to –4.9 kcal/mol for chitosan-5 FU complex.

Chitosan also demonstrated an acceptable binding affinity for both LOR and 5-FU. However, the Gibbs free energy was lower, indicating a lower affinity for drugs than zein. Hence, zein was selected for further in silico visualization before being incorporated into the design of the polymeric nanocarriers for this study.

Molecular docking analysis showed that zein is capable of forming stable interactions with both LOR and 5-FU, confirming its high efficiency as a dual-drug nanocarrier system. It is inferred that LOR was successfully incorporated within the hydrophobic cavity of the zein structure, where stabilization was observed through π–π stacking with PHE:A137, π–alkyl interactions with ALA:A151, VAL:A133, and LEU:A146, and hydrogen bonding with both GLN:A140 and GLN:A143. These detected non-covalent forces collectively explain the strong affinity of LOR towards zein's non-polar cavities, resulting in sustained and prolonged release.

On the contrary, 5-FU exhibited high binding affinity with zein structure through electrostatic and hydrogen-bonding interactions, such as salt bridges with GLU:A145 and hydrogen bonds with GLN:A140, ARG:A91, and LEU:A146. The dual functionality of zein to interact with both LOR and 5-FU each with different mechanism renders it a potential amphiphilic nanocarrier system capable of accommodating both hydrophobic and hydrophilic drugs.

Preliminary screening showed that the properties of FU-ZN/TAN nanoparticles were significantly influenced by both the processing method and the volume of aqueous phase volume. In other words, both homogenization and probe sonication showed noticeable enhancement in particle size uniformity as well as entrapment efficiency as observed in F1, it exhibited the smallest particles size (388 nm), lowest PDI (0.345), while the highest EE% (90.6%). On the other hand, formulations prepared without using homogenization and probe sonication displayed broader size distributions with lower encapsulation efficiency, confirming the efficiency of both techniques to preserve good dispersion and nucleation during nanoparticle preparation. Furthermore, increased volume of the aqueous phase volume, as seen in F3–F4 resulted in formation of larger particle sizes with higher PDIs. This could be attributed to slower precipitation kinetics or minimized supersaturation. However, all tested formulations exhibited a high negatively surface charge (−21 to −25 mV),

confirming their stability through electrostatic repulsion forces inhibiting their aggregation. Overall, F1 was selected as the most potential formulation for further optimization through Box–Behnken design.

Box–Behnken designed successfully detected the formulation parameters influencing the physicochemical properties of both LOR-ZN/TAN and FU-ZN/TAN nanoparticles. For instance, both ZN and LOR amounts were determined as the main factors affecting the particle size of LOR-ZN/TAN NPs, where increasing zein amount was found to increase nanoparticles size proportionally owing to increased ZN aggregation during nanoformulation. In contrast, higher amounts of LOR led to the observed reduction in particle size. This is attributed to the LOR hydrophobic interaction with zein non-polar cavities, due to more intense molecular interactions. The obtained strong quadratic effect of LOR amount confirmed a nonlinear reduction behavior, highlighting LOR molecular role in controlling nanoparticles formulation. Similarly, zein and 5-FU were found to influence FU-ZN/TAN NPs size, where larger amounts of both zein and 5-FU were accompanied by larger nanoparticles. However, tannic acid amount was found to exhibit significant inverse influence on nanoparticles size, owing to its high crosslinking ability with zein forming complex matrices limiting particle size increase. Moderate to high negative surface charges recorded in the range of −6.8 to −27.8 mV indicate that the prepared systems are stabilized forming dispersed formulations with minimal aggregation liability due to the repulsion forces. Overall, the experimental design results confirm the high capability of ZN/TAN NPs as potential tolerable biocompatible carrier systems for the co-delivery of both hydrophobic and hydrophilic drugs.

TEM images confirmed the successful formation of both LOR-ZN/TAN and FU-ZN/TAN NPs, showing uniform, almost spherical nanoparticles. TEM images reveal smaller nanoparticles size compared to DLS measurements. This is attributed to the presence of a hydration layer surrounding the nanoparticles in the nanosuspension samples measured by DLS which detect the hydrodynamic diameters of nanoparticles within their suspensions. This observation is in a good agreement with previously reported studies confirming that the apparent larger size of polymeric nanoparticles determined by DLS compared to that determined by TEM returns back to Brownian motion and solvent association.

FTIR analysis also confirmed the successful formation of nanoparticles as well as drug incorporation. First, characteristic amide I (~1650 cm^{-1}) and amide II (~1550 cm^{-1}) peaks observed in zein structure, as well as the O–H and C=O vibrations of tannic acid, were found to be shifted and broadened within the spectra of ZN/TAN nanoparticles, highlighting the strong hydrogen bonding between the hydroxyl groups of the phenolic structure of TAN and the amide groups within zein structure. Furthermore, LOR-ZN/TAN spectrum exhibited C–H stretching band (2750–2850 cm^{-1}) attributing to LOR structure confirming its incorporation within the hydrophobic domains of zein. Similarly, FU-ZN/TAN NPs showed characteristic peaks of C–F and C=O attributing to 5-FU structure (1300–1700 cm^{-1}), indicating the molecular interactions between the drug and ZN/TAN NPs. The partial reduction of peaks intensity of both drugs verifies the successful of their incorporation within the protein-phenol matrices. Overall, both the morphological and spectroscopic characterization confirm the successful formation of uniform ZN/TAN NPs capable of incorporating both hydrophobic and hydrophilic drugs through various interactions.

Both LOR and 5-FU demonstrated showed programmed controlled release profile out of their corresponding ZN/TAN NPs. Free LOR showed complete release within only 8 hours, while LOR-ZN/TAN nanoparticles exhibited extended release up to 24 hours, marked by an initial burst release of around ~30% of the initial incorporated amount followed by a slower diffusion-sustained phase, fitting with the Korsmeyer–Peppas model ($r^2 = 0.991$). Similarly, free 5-FU showed a complete release pattern within only 6 hours, while FU-ZN/TAN NPs exhibited a more sustained and controlled release pattern over 48 hours, with an initial burst of around ~22% of the initial incorporated amount. This was supported by a strong correlation to the Korsmeyer–Peppas model ($r^2 = 0.981$). The relatively slower release behavior of 5-FU compared to LOR is in good agreement with its stronger binding affinity to zein compared to LOR. Overall, molecular docking along with entrapment efficiency studies confirm the high potentiality of ZN/TAN NPs as controlled and sustained delivery system for both hydrophobic and hydrophilic drugs.

The cytotoxic and cell cycle analysis confirmed the improved anticancer efficacy of ZN/TAN NPs, when loaded with LOR and 5-FU. All tested nanoformulations showed dose-dependent cytotoxicity toward MCF-7 breast cancer cells. However, FU-ZN/TAN NPs recorded the highest inhibitory effect, surpassing free 5-FU. This returns back to their enhanced cellular internalization and sustained drug release compared to free drug. On the contrary, LOR-ZN/TAN NPs exhibited moderate cytotoxicity, which matches their controlled-release profile. Interestingly, the 1:1 mixture of LOR-

ZN/TAN NPs and FU-ZN/TAN NPs were found to induce cytotoxicity efficacy comparable to FU-ZN/TAN NPs alone although containing only half dose of 5-FU. This suggests the potential synergistic activity between LOR and 5-FU that offers a capability of dose reduction while maintaining the required efficacy.

Apoptosis analysis by flow cytometry confirmed that FU-ZN/TAN NPs induced high apoptotic index (≈37%), suggesting their capability to induce programmed cell death through sustained intracellular drug availability. The mixed 1:1 ratio of both nanoparticle formulations also triggered both substantial early and late apoptosis, almost mimicking that of FU-ZN/TAN NPs. This was also accompanied by minimal necrosis, suggesting that the co-delivery system preferentially induces apoptotic pathways rather than necrotic pathways which are considered as an advantageous feature for anticancer therapeutic agent.

Cell-cycle analysis further presented complementary mechanisms, where FU-ZN/TAN NPs showed noticeable S-phase arrest (≈51%), matching the reported 5-FU mechanism of DNA synthesis blockage and thymidylate synthase inhibition. In contrast, LOR-ZN/TAN NPs primarily arrested cells in the G0/G1 phase (≈54%), reflecting the reported mechanism of LOR to modulate checkpoint kinases and suppress CDC25-CDK1 signaling. Interestingly, the combined 1:1 ratio of the combined LOR-ZN/TAN NPs and FU-ZN/TAN NPs showed a balanced dual-phase blockade – G0/G1 and S phase resulting in impeding DNA replication and cell-cycle progression, respectively. Although LOR-ZN/TAN NPs showed the highest cells proportion in the G_0/G_1 phase, the difference compared to the unloaded ZN/TAN NPs was found to be moderate, confirming that tannic acid exhibits a significant role in inducing early cell-cycle arrest. Finally, these results reveal that the hybrid formulation of both loaded nanoparticles presents a potential synergistic activity through controlled release behavior, improved apoptosis, and dual-mechanism cell-cycle arrest, presenting a promising safer anti-cancer therapy for breast cancer management.

Conclusion

This study demonstrated the successful formulation of ZN/TAN NPs for the combinatorial incorporation of LOR and 5-FU as a potential antiproliferative therapy for breast cancer management for the purpose of reducing the required doses and minimizing the associated adverse effects. The optimized nanoparticles exhibited uniform dispersion of NPs of ≈200–230 nm, and sustained drug release monitored over 24–48 hours. Various nanoparticle formulations were optimized using a Box-Behnken experimental design using the Design Expert® software. The Optimized LOR-ZN/TAN NPs had a particle size of 197 nm, PDI of 0.153, zeta potential of –21.78 mV, and entrapment efficiency of 61.33%. Furthermore, FU-optimized ZN/TAN NPs had a particle size of 231 nm, 0.170 for PDI, of 24.01 mV, and entrapment efficiency of 74.91%. The results showed a low bias% compared to the values predicted by the software, validating the reliability of the chosen model.

In vitro cell studies in MCF-7 breast cancer cells showed that the combination of LOR-ZN/TAN and FU-ZN/TAN NPs induced dual mechanisms in breast cancer therapy by targeting both early cell cycle arrest and DNA synthesis inhibition, confirming their potential as promising nanocarrier systems for promoting the therapeutic efficacy of both drugs in breast cancer management. For instance, cytotoxicity and flow-cytometry analyses in MCF-7 cells showed enhanced apoptotic activity and dual cell-cycle arrest upon the combination of the two drug-loaded NPs, indicating an additive anticancer activity.

While these results support the potential of a ZN/TAN NPs for the co-delivery of LOR and 5-FU, various limitations should be recognized for future studies. Hence, the current work is counted as a proof-of-concept proving the combinatorial anti-cancer potential of LOR and 5-FU loaded ZN/TAN NPs. Future studies will focus on evaluating molecular pathways (cyclin/CDK modulation), as well as studying pharmacokinetic analyses in animal models to confirm potentiality of translational relevance.

Data Sharing Statement

The data presented in this study are available on request from the corresponding author (Moawia M Al-Tabakha).

Acknowledgments

The authors extend their appreciation to the Deanship of Graduate Studies at Ajman University, Ajman, United Arab Emirates, for their publication support.

Author Contributions

All authors made a significant contribution to the work reported, whether that is in the conception, study design, execution, acquisition of data, analysis and interpretation, or in all these areas; took part in drafting, revising or critically reviewing the article; gave final approval of the version to be published; have agreed on the journal to which the article has been submitted; and agree to be accountable for all aspects of the work.

Funding

This research was supported by the Ajman University Internal Research Grant No. DGSR Ref.2022-IRG-PH-7. The authors are solely responsible for the research findings presented in this paper.

Disclosure

The authors declare that they have no known competing financial interests or personal relationships that could influence the work reported in this study.

References

1. Siegel RL, Miller KD, Jemal A. Cancer statistics, 2020. *Ca A Cancer J Clin*. 2020;70:7–30. doi:10.3322/caac.21590
2. Grayson M. Breast cancer. *Nature*. 2012;485:S49. doi:10.1038/485S49a
3. Bray F, Ferlay J, Soerjomataram I, et al. Global cancer statistics 2018: GLOBOCAN estimates of incidence and mortality worldwide for 36 cancers in 185 countries. *Ca A Cancer J Clin*. 2018;68:394–424. doi:10.3322/caac.21492
4. Ali IH, Al-Tabakha MM, Khalil IA. Loratadine loaded chitosan tannic acid nanoparticles as anti-proliferative agent against breast cancer: in-silico, in-vitro and cell studies. *Int J Nanomed*. 2024;Volume 19:12483–12504. doi:10.2147/IJN.S483667
5. Soule BP, Simone NL, DeGraff WG, et al. Loratadine dysregulates cell cycle progression and enhances the effect of radiation in human tumor cell lines. *Radiat Oncol*. 2010;5(1):1–12. doi:10.1186/1748-717X-5-8
6. Simon FER, Simons KJ. H1 antihistamines: current status and future directions. *World Allergy Organ J*. 2008;1:145–155. doi:10.1186/1939-4551-1-9-145
7. Blaya B, Nicolau-Galmes F, Jangi S, et al. Histamine and histamine receptor antagonists in cancer biology. *Inflamm Allergy Drug Targets*. 2010;9 (3):146–157. doi:10.2174/187152810792231869
8. Wang WT, Chen Y-H, Hsu J-L, et al. Terfenadine induces anti-proliferative and apoptotic activities in human hormone-refractory prostate cancer through histamine receptor-independent Mcl-1 cleavage and Bak up-regulation. *Naunyn-Schmiedeberg's Arch Pharmacol*. 2014;387:33–45. doi:10.1007/s00210-013-0912-x
9. Chen J-S, Lin S-Y, Tso W-L, et al. Checkpoint kinase 1-mediated phosphorylation of Cdc25C and bad proteins are involved in antitumor effects of loratadine-induced G 2 /M phase cell-cycle arrest and apoptosis. *Mol Carcinogenesis*. 2006;45:461–478. doi:10.1002/mc.20165
10. Christensen S, Van der Roest B, Besselink N, et al. 5-Fluorouracil treatment induces characteristic T>G mutations in human cancer. *Nat Commun*. 2019;10:1–11. doi:10.1038/s41467-019-12594-8
11. Hassan EA, Hathout RM, Gad HA, Sammour OA. A holistic review on zein nanoparticles and their use in phytochemicals delivery. *J Drug Delivery Sci Technol*. 2022;73:103460. doi:10.1016/j.jddst.2022.103460
12. Liu G, An D, Li J, Deng S. Zein-based nanoparticles: preparation, characterization, and pharmaceutical application. *Front Pharmacol*. 2023;14:1120251.
13. Liu X, Zhang M, Zhou X, et al. Research advances in Zein-based nano-delivery systems. *Front Nutr*. 2024;11:1379982.
14. Chen H, Zhang Y, Zhong Q. Physical and antimicrobial properties of spray-dried zein-casein nanocapsules with co-encapsulated eugenol and thymol. *J Food Eng*. 2014;144:93–102. doi:10.1016/j.jfoodeng.2014.07.021
15. Li M, Yu M. Development of a nanoparticle delivery system based on zein/polysaccharide complexes. *J Food Sci*. 2020;85:4108–4117. doi:10.1111/1750-3841.15535
16. Booth BW, Inskeep BD, Shah H, et al. Tannic acid preferentially targets estrogen receptor-positive breast cancer. *Int J Breast Cancer*. 2013;2013:1–9. doi:10.1155/2013/369609
17. Losso JN, Bansode RR, Trappey A, Bawadi HA, Truax R. In vitro anti-proliferative activities of ellagic acid. *J Nutr Biochem*. 2004;15:672–678. doi:10.1016/j.jnutbio.2004.06.004
18. Boitier E, Gautier JC, Roberts R. Advances in understanding the regulation of apoptosis and mitosis by peroxisome-proliferator activated receptors in pre-clinical models: relevance for human health and disease. *Comparat Hepatol*. 2003;2(3). doi:10.1186/1476-5926-2-3
19. Bawadi HA, Bansode RR, Trappey A, Truax RE, Losso JN. Inhibition of Caco-2 colon, MCF-7 and Hs578T breast, and DU 145 prostatic cancer cell proliferation by water-soluble black bean condensed tannins. *Cancer Lett*. 2005;218:153–162. doi:10.1016/j.canlet.2004.06.021
20. Stennicke HR, Renatus M, Meldal M, Salvesen GS. Internally quenched fluorescent peptide substrates disclose the subsite preferences of human caspases 1, 3, 6, 7 and 8. *Biochem J*. 2000;350:563–568. doi:10.1042/bj3500563

21. Thornberry NA, Rano TA, Peterson EP, et al. A combinatorial approach defines specificities of members of the caspase family and granzyme B. Functional relationships established for key mediators of apoptosis. *J Biol Chem*. 1997;272(29):17907–17911. doi:10.1074/jbc.272.29.17907
22. Bienert S, Waterhouse A, de Beer T, et al. The Swiss-MODEL repository-new features and functionality. *Nucleic Acids Res*. 2017;45:D313–D319. doi:10.1093/nar/gkw1132
23. Waterhouse AL, Bertoni M, Bienert S, et al. Swiss-MODEL: homology modelling of protein structures and complexes. *Nucleic Acids Res*. 2018;46 (W1):W296–W303. doi:10.1093/nar/gky427
24. Liu Y, Grimm M, Dai W-T, et al. CB-Dock: a web server for cavity detection-guided protein–ligand blind docking. *Acta Pharmacologica Sinica 2019*. 2019;41(1):138–144. doi:10.1038/s41401-019-0228-6
25. Liang X, Cao K, Li W, et al. Tannic acid-fortified zein-pectin nanoparticles: stability, properties, antioxidant activity, and in vitro digestion. *Food Res Int*. 2021;145:110425. doi:10.1016/j.foodres.2021.110425
26. Abo-zalam HB, El-Denshary ES, Abdelsalam RM, et al. Therapeutic advancement of simvastatin-loaded solid lipid nanoparticles (SV-SLNs) in treatment of hyperlipidemia and attenuating hepatotoxicity, myopathy and apoptosis: comprehensive study. *Biomed Pharmacother*. 2021;139:111494. doi:10.1016/j.biopha.2021.111494
27. Shah M, Pathak K. Development and Statistical Optimization of Solid Lipid Nanoparticles of Simvastatin by Using 2 3 Full-Factorial Design. *AAPS Pharm Sci Tech*. 2010;11:489–496. doi:10.1208/s12249-010-9414-z
28. Agnihotri SA, Jawalkar SS, Aminabhavi TM. Controlled release of cephalexin through gellan gum beads: effect of formulation parameters on entrapment efficiency, size, and drug release. *Eur J Pharm Biopharm*. 2006;63:249–261. doi:10.1016/j.ejpb.2005.12.008
29. Costa P, Sousa Lobo JM. Modeling and comparison of dissolution profiles. *Eur J Pharm Sci*. 2001;13:123–133. doi:10.1016/S0928-0987(01) 00095-1
30. Ibrahim A, Khalil IA, El-Sherbiny IM. Development and evaluation of core-shell nanocarrier system for enhancing the cytotoxicity of doxorubicin/ metformin combination against breast cancer cell line. *J Pharmaceut Sci*. 2022;1–11. doi:10.1016/j.xphs.2022.05.018
31. Ali IH, Khalil IA, El-Sherbiny IM. Single-dose electrospun nanoparticles-in-nanofibers wound dressings with enhanced epithelialization, collagen deposition, and granulation properties. *ACS Appl Mater Interfaces*. 2016;8. doi:10.1021/acsami.6b04369
32. Khalil IA, Ali IH, El-Sherbiny IM. Noninvasive biodegradable nanoparticles-in-nanofibers single-dose ocular insert: in vitro, ex vivo and in vivo evaluation. *Nanomedicine*. 2019;14:33–55. doi:10.2217/nnm-2018-0297
33. Betancourt T, Brown B, Brannon-Peppas L. Doxorubicin-loaded PLGA nanoparticles by nanoprecpitation: preparation, characterization, and in-vitro evaluation. *Future Med*. 2007;2:219–232.
34. Delan WK, Ali IH, Zakaria M, et al. Investigating the bone regeneration activity of PVA nanofibers scaffolds loaded with simvastatin/chitosan nanoparticles in an induced bone defect rabbit model. *Int J Biol Macromol*. 2022;222:2399–2413. doi:10.1016/j.ijbiomac.2022.10.026
35. Hassan FE, Aboulhoda BE, Ali IH, et al. Evaluating the protective role of trimetazidine versus nano-trimetazidine in amelioration of bilateral renal ischemia/reperfusion induced neuro-degeneration: implications of ERK1/2, JNK and Galectin-3 /NF-κB/TNF-α/HMGB-1 signaling. *Tissue Cell*. 2023;85:102241. doi:10.1016/j.tice.2023.102241
36. Monfared A, Ghaee A, Ebrahimi-Barough S. Preparation and characterisation of zein/polyphenol nanofibres for nerve tissue regeneration. *IET Nanobiotechnol*. 2019;13:571–577. doi:10.1049/iet-nbt.2018.5368
37. Lv W-T, Liu -X-X, Dai X-L, Long X-T, Chen J-M. A 5-fluorouracil–kaempferol drug–drug cocrystal: a ternary phase diagram, characterization and property evaluation. *CrystEngComm*. 2020;22:8127–8135. doi:10.1039/D0CE01289K
38. Kurebayashi J, Kanomata N, Kozuka Y, et al. The cell cycle profile test is a prognostic indicator for breast cancer patients treated with postoperative 5-fluorouracil-based chemotherapy. *Jpn J Clin Oncol*. 2011;41(6):739–746. doi:10.1093/jjco/hyr042